Chapter 3

The Use of Fiber Reinforced Plastic for The Repair and Strengthening of Existing Reinforced Concrete Structural Elements Damaged by Earthquakes

George C. Manos and Kostas V. Katakalos

Additional information is available at the end of the chapter

http://dx.doi.org/10.5772/51326

1. Introduction

During the last fifty years various parts of the world have been subjected to a number of damaging earthquakes. Greece is one of the countries where such damaging earthquakes occur quite frequently ([1]). Some of these earthquakes, not necessarily the most intense, occurred near urban areas and thus subjected various types of structures to significant earthquake forces leading to damage ([2]). For some of these earthquakes, ground motion acceleration recordings were obtained at distances relatively close to the area of intense shaking, thus providing valuable information for correlating the observed damage with this ground motion recording and its characteristics. Moreover, following the most damaging of these earthquakes, studies were initiated that led to the revision of the provisions of Seismic Codes [3]. The damaged structures included old structural formations, sometimes older than one hundred years, which were not designed for seismic forces. They usually belong to cultural heritage and are under various forms of conservation status that does not allow all types of retrofitting but only retrofitting materials and techniques that are compatible with the existing materials; moreover, the applied retrofitting in these cases must also be reversible so that it can be easily removed in case it demonstrates undesirable effects with time. Apart from the cultural heritage structures, the damaged structures also include relatively contemporary structures that are usually less than fifty years old. The vast majority of these structures are multistory reinforced concrete (R/C) buildings. There are other types of structures apart from (R/C) buildings, such as structures forming the infrastructure or industrial facilities which can also develop earthquake damage. However, this chapter will be devoted to the usual R/C residential multi-story buildings, the earthquake damage of their structural elements and their strengthening.

1.1. Damage observations for contemporary R/C structures

These structures are usually designed and built according to the provisions of a Seismic Code ([3]). The cause of damage may be due to:

The code provisions underestimating the severity of the shaking and thus underestimating the seismic demand posed upon the various structural elements, their connections and the foundation of the whole structure.

The code provisions together with the specification of the materials resulting in such strengths that are below the seismic demands placed upon the structural elements.

The detailing and the realization of the design during construction or alteration during the life time of the building resulting again in such strengths for the various structural elements that are below the corresponding seismic demands placed upon them.

In all cases the appearance of structural damage results from the above fundamental causes, either from one of them or from their combination; this is expressed by the following inequality (Eq. 1) between the strength and the demand put upon the various members of the structural system, whereby the demand is signified as S_d and the strength as R_d. Damage is expected to occur when this inequality is not satisfied [4].

$$S_d < R_d \tag{1}$$

A serious task, after a strong earthquake affects an urban area, is to appraise the severity of the structural damage for a large number of buildings. This is usually done in Greece by engineers specially appointed for this task by the Government. The screening process commences a few days after the natural disaster, provided that the seismic sequence has subsided. There are certain guidelines published by the Hellenic Organization of Earthquake Planning and Protection to facilitate the appointed engineers in this damage screening process [5]. In general terms the first round of inspection must lead to the classification of each building to one of the three main categories. The first damage category is that there is no structural damage and the mainly non-structural damage does not pose any danger; so these buildings can be reused immediately. The second damage category is that there is non-structural damage as well as some structural damage; the latter, although contained, may have led to a considerable decrease of the bearing seismic capacity of the damaged structural elements and the structure as a whole. There may be need for temporary shoring and the removal of dangerously damaged non-structural elements. These buildings will be subjected to a second round of inspection after these countermeasures have been accomplished. Their reuse will be decided after the second round of screening. The third category includes buildings with relatively extensive damage to its structural elements (slabs, beams, columns or shear walls) [5], [6]; the damage is relatively widespread in terms of story level. Permanent deformations of the structural elements are evident in the form of concrete cracking and crushing in certain critical areas of the structural elements indicating that these areas have been overstressed and inequality 1 has ceased to be valid. There is serious consideration that this bearing seismic capacity reduction may lead to partial collapse. There may be urgent

http://dx.doi.org/10.5772/51326

need for temporary shoring and the removal of dangerously damaged parts in order to avoid, if possible, partial collapse (figure 1b). These buildings will also be subjected to a second round of inspection. If it is decided that they pose a public threat, due to the possibility of partial or total collapse, they should be demolished (figure 1a); otherwise, a special design should devise a feasible scheme for their repair and strengthening. The following sections will address the task of repair and strengthening of structural elements that have been subjected to such earthquake damage to their structural system and have been classified as belonging to the second or third seismic damage categories after the second round of screening process.

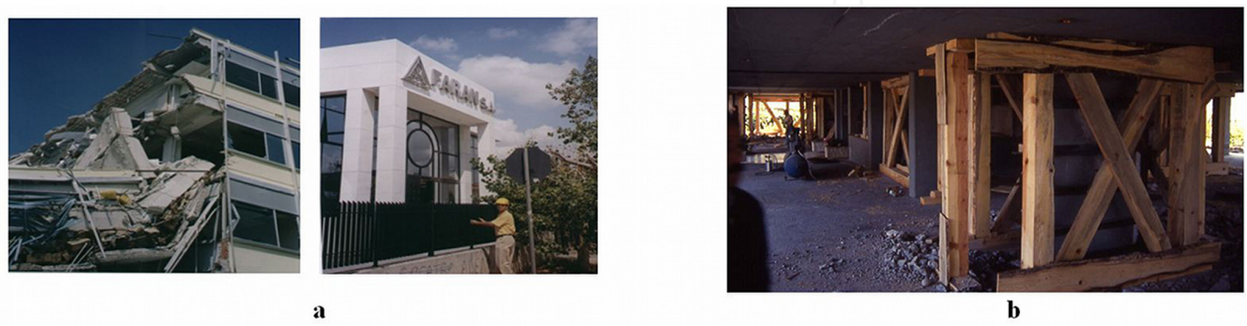

Figure 1. a The old building of a pharmaceutical company that collapsed during the Athens 1999 earthquake together with an upgraded building next to it that survived unscathed [2]. b. Temporary shoring of 4-story building (Hardas) damaged during the Pyrgos 1993 earthquake [2].

1.2. Structural damage description at the level of the structural element

It is usual to describe the structural damage at the level of each reinforced concrete structural member, e.g. slab, beam, column and shear wall, always having in mind inequality 1 and the fact that the axial (N), bending (M) and shear (Q) force demands in each one of these structural members from the combination of dead and live loads plus the earthquake forces are of a particular nature. Thus, for the slabs the demands are mainly flexural whereas for the beams the demands are flexural and shear. For the columns the demands are flexural and shear with the presence of considerable axial forces whereas for the shear walls the demands are flexural and shear with the presence of a relatively lower level of axial forces than that of the columns. Apart from the structural elements themselves, one should also consider critical areas of their connections (joints) as well as the foundation. Both, the structural connections and the foundation are very critical areas that require special consideration in both identifying the nature of the structural damage as well as proposing countermeasures. This presentation does not deal with either of these critical areas. The main flexural structural damage in slabs and beams develops in the areas of maximum bending moments. For the beams they usually develop near the joints with the columns and shear walls (figure 2a) where large bending moments are expected to develop from the seismic forces. Similarly, at the ends of the beams are the areas of large shear forces from the combination of earthquake forces with the dead and live loads; these will cause the appear-

ance of shear damage in the form of diagonal cracks (figure 2a). The presence of large bending moments mainly from the seismic load together with large axial forces will cause the formation of flexural damage at the top and the toe of columns (see figure 2b) whereas the presence of shear forces from the seismic loads together with axial forces will lead to the formation of shear damage at the columns (see figure 2c). The presence of large shear forces from seismic loads together with relatively low level axial forces will lead to the development of shear damage in the shear walls (see figure 3a) whereas the presence of short columns will lead to the development of large shear forces from seismic loads and the development of shear damage as shown in figure 3b.

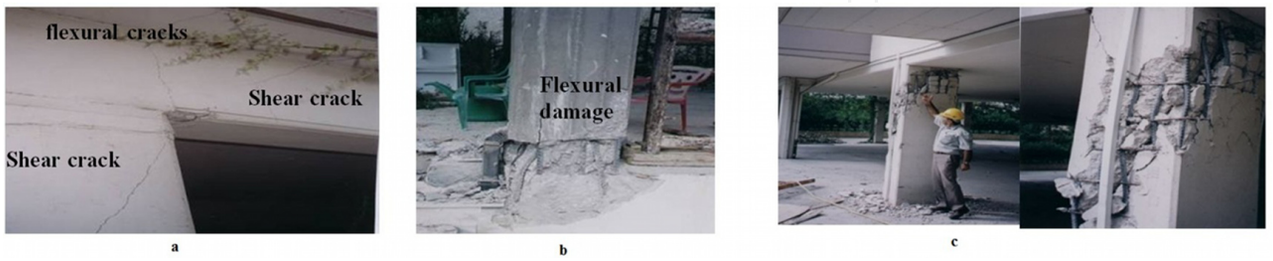

Figure 2. a Typical damage of beam at the joint with the nearby column (6th story building, Aharnes, Athens earthquake 1995), [2]. b Typical damage of the toe of a column at ground floor (two-story building, Nea Kifisia,, Athens earthquake 1995), [2]. c Typical shear damage at the columns of a "soft story" (4-story Metamorfosi building, Athens earthquake 1995), [2].

1.3. The strategy for the repair and strengthening scheme

In the previous discussion the emphasis in the description of damage was on attributing the various forms of structural damage to the nature of the demand (either flexural or shear with or without axial forces). However, as already stressed by inequality 1, structural damage is due to the fact that the said demand was not met by the existing strength. The strategy for retrofitting damaged structural systems, or structural systems that can be demonstrated by analytical methods prior to a strong earthquake to be prone to potential damage in the future, must be based on either somehow lowering the demands or increasing the corresponding strengths or both. In an effort to lower the demands, one can try to decrease the masses mobilized by the earthquake vibrations. This can be accomplished either by removing unnecessary mass or by changing the structural system in such a way that the resulting dynamic system combined with the design spectrum leads to a decrease in the earthquake loads (e.g. seismic isolation). Lowering the demands in the way described before is not always feasible. Thus, the retrofitting scheme is usually based on increasing the strengths of the structural members. In doing so, one must be aware that it is advisable to increase the deformability of the structural members thus increasing the ability of the structural system to dissipate the seismic energy through plastic deformations that are designed to develop at predetermined locations ([7], [8] [9], [10]). The location where these plastic deformations occur should be such that it does not lead to unstable structural formations. Sometimes, a partial objective of the strengthening scheme is to increase the stiffness to a moderate degree,

http://dx.doi.org/10.5772/51326

especially for structural systems that can develop excessive torsional response. However, frequently a considerable increase in the stiffness of the strengthened structural system results as an indirect consequence of the adopted scheme whereas its main objectives were to increase the strength and deformability of the structural elements and of the structure as a whole. This increase in stiffness results in larger demands due to the dynamics of the strengthened structure, as it corresponds to higher amplitudes of design spectral accelerations than the un-strengthened structural system. This is usually the case when traditional strengthening schemes are employed utilizing reinforced concrete jacketing of the structural members (columns and beams) or the addition of shear walls by encasing reinforced concrete elements within the bays of the corresponding R/C frames [6]. The strengthening schemes that can be employed in order to increase the flexural or shear capacity of columns, beams or shear walls utilizing fiber reinforcing plastics (FRP) usually made of carbon, glass or steel do not result in this undesirable increase in stiffness. Moreover, due to their external application, they usually require less interference with or breaking of the volume of existing R/C structural elements. Finally, such strengthening schemes become effective in a much shorter time than traditional strengthening schemes ([11], [12], [13], [14], [15], [16]).

Figure 3. a Typical damage of shear walls at the "soft story" during The Kozani 1995 Earthquake in Greece. b. Typical damage of "short" columns during The Kozani 1995 Earthquake in Greece.

2. Main applications for dealing with earthquake structural damage utilizing fiber reinforcing plastics

In section 1.2 a brief description of earthquake structural damage that usually develops in slabs, beams, columns or shear walls of multi-story R/C buildings was presented. In this section, the use of fiber reinforcing plastics (FRP) will be discussed in a way dealing with the corresponding damage. These FRP materials behave in tension almost elastically till their ultimate state that for the material itself is the breaking of the fibers in tension; they do not develop any forces in shear or compression. The value for the modulus of elasticity is approximately 240Gpa for carbon fibers, 200Gpa for steel fibers and 80Gpa for glass fibers ([8], [17]).

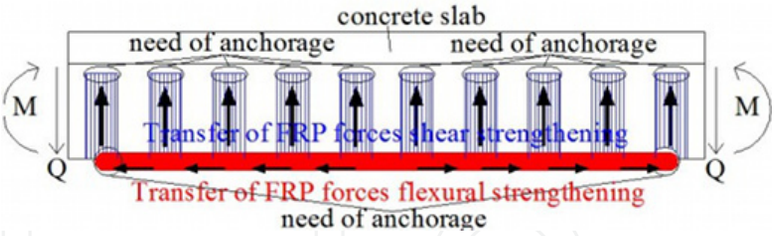

Figure 4. Flexural and shear FRP reinforcement for a T-beam.

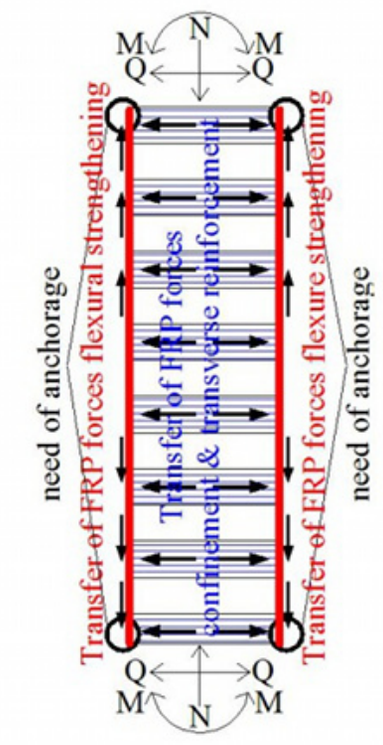

Figure 5. Flexural and shear FRP reinforcement for a column.

The ultimate axial strain values given by the manufacturers reach values in the range of 2%. Consequently, sheets made by these materials, despite their relatively small thickness which is usually below 0.2mm for one layer, can develop substantial tensile forces in the direction of their fibers (see figures 4 and 5). This property accompanied with their low weight and the very easy external application to structural elements, by attaching them on the external surfaces by proper organic or inorganic matrices, results in their being used as effective longitudinal or transverse reinforcement for such structural elements that are in need of strengthening (see figures 4, 5 and [12], [15], [16]). However, the following limitations exist for this type of application. The first limitation springs from the fact that the ultimate axial strain value of the order of 2% for the material of the fiber cannot be reached for all the fibers together in a sheet due to the actual conditions of the attachment that results in non-

http://dx.doi.org/10.5772/51326

uniform distribution of the strain field ([13], [18], [19]). Thus, for design purposes, the adopted limit axial strain value is usually below ½ of the ultimate axial strain value for the fiber material. The second limitation results from the way the tensile forces which develop on these FRP sheets can be transferred. When the transfer of these forces relies solely on the interface between the FRP sheet and the external surface of the reinforced concrete structural elements, the delamination (debonding) mode of failure of these sheets occurs, due to the relatively low value of either the ultimate bond stress at this interface or the relatively low value of the tensile strength of the underlying concrete volume. This mode of failure is quite common and it occurs in many applications well before the corresponding FRP sheets develop tensile axial strains in the neighborhood of values mentioned before as design limit axial strains (approximately of the order of 1%). Consequently, there is need of alternative ways in order to transfer these tensile forces apart from the simple attachment, in order to enhance the exploitation of the FRP material potential. This will be presented and discussed in the following paragraphs ([11], [13], [20], [21], [22], [23]).

2.1. Upgrading the flexural capacity of slabs

The main cause of damage in this case is the fact that the flexural capacity cannot meet the demand. Fiber reinforced plastics either in the form of sheets or laminates are externally attached to the slab either at the top or at the bottom surface (positive or negative bending moment demand). Such a scheme was utilized in the upgrading of the seismic capacity of the slabs of a 4-story R/C building built in 1933 and subjected to the Kozani, 1995 earthquake in Greece ([2], [24]). For this strengthening scheme it was planned to make use of a certain type of Carbon Fiber Reinforcing Plastic laminates (CFRP) with a cross-section 50mm x 1.2mm. These laminates could be applied in-situ either on the upper or lower surface of the concrete slabs with the use of a special epoxy paste. An extensive experimental parametric study was performed on this type of attachment by testing a series of specimens prior to applying the best attachment detail to prototype slab specimens. The tests were performed at the laboratory of Strength of Materials of Aristotle University and utilized twin prismatic concrete specimens with dimensions 100mm x 100mm x 150mm each. These twin concrete prisms were joined with these CFRP laminates; they were attached on the two opposite sides of each twin concrete prism. These specimens were then subjected to such a loading as would force the laminates to be detached from the concrete surface. This is shown in figures 6a to 6d. A variety of attachments between the CFRP laminates and the twin concrete prisms were tried. The simplest form of attachment was the one employing only epoxy paste between the CFRP laminates and the concrete surface (figures 6a and 6b). Next, a variety of bolting arrangements were utilized with or without the epoxy paste. Figures 6c and 6d depict such an attachment of the laminates whereby the epoxy paste is combined with one bolt on each side of the twin concrete prism. The bond strength in the first case was found equal to 2.70Mpa whereas in the second case equal to 4.40Mpa, which represents an increase of 63%. The maximum bond strength that was achieved throughout these tests reached the value of 7.20Mpa, which represents an increase of 167% from the simple attachment of the laminates only with epoxy paste. These findings were utilized with slab specimens that were

taken from the actual mezzanine slab of the prototype structure; they were cut from parts of the slab where an opening would be formed for a new staircase.

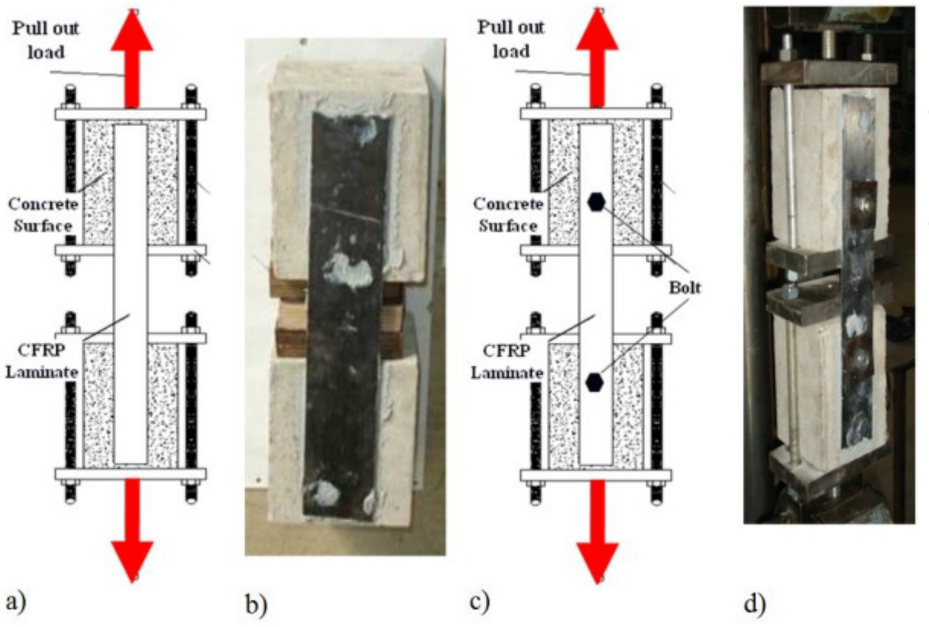

Figure 6. Bond tests of the used CFRP laminates

Figure 7. Loading arrangement of the slab specimens in flexure.

http://dx.doi.org/10.5772/51326

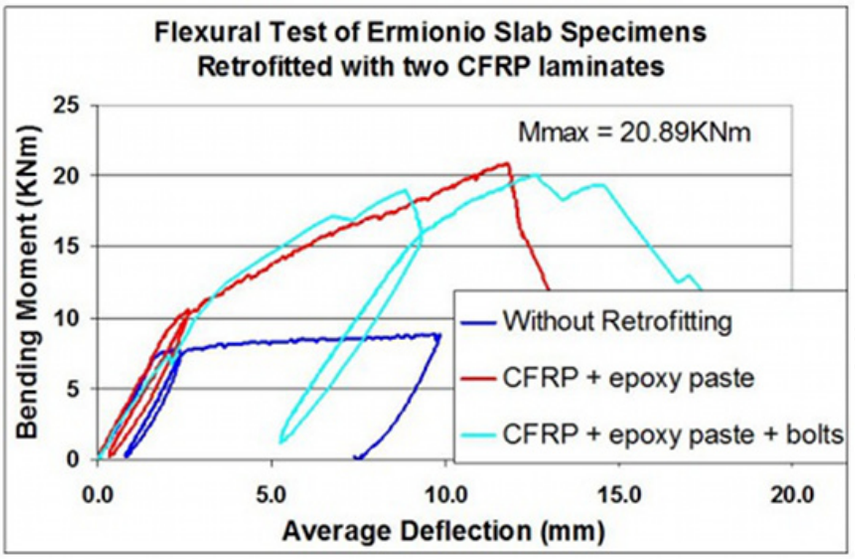

Figure 8. Flexural behavior of Ermionio slab specimen retrofitted with two CFRP laminates either bonded only with epoxy paste or with epoxy paste and bolts.

Figure 9. Flexural failure of the Ermionio slab specimen retrofitted with two CFRP laminates bonded only with epoxy paste. The CFRP laminates were debonded from the concrete slab in this case.

Figure 7 depicts the loading arrangement that was used to subject these slab specimens to four-point flexure. Initially, this was done for a specimen without any retrofitting that reached a maximum bending moment value equal to 8.84KNm. Then two laminate strips, each having a cross section of 50mm x 1.2mm, were attached on the bottom surface of this slab specimen, which was reloaded to flexure as before. Figure 8 depicts the obtained flexural behavior of this retrofitted slab specimen. At this stage, the CFRP laminates were attached to the specimen only with the use of epoxy paste. This time the specimen reached a maximum bending moment value equal to 20.89KNm, which represents an increase equal to

136% when compared to the maximum bending moment value of the un-retrofitted slab. This retrofitted slab failed in the form of the debonding of the CFRP laminates (figure 9). The debonding of the two CFRP laminates was followed by a sharp decrease in the flexural bearing capacity together with the formation of a plastic hinge at mid-span in the form of excessive plastic deformations of the old steel reinforcing bars at the bottom of the slab as well as crushing of the concrete at the top of the slab. Next, two new CFRP laminates were reattached to the same slab specimen; this time epoxy paste was used again together with bolts penetrating through the slab and securing the attachment of these CFRP laminates. The flexural bearing capacity of the slab this time reached the same maximum bending moment value as the one observed when only epoxy paste was used for the attachment of the laminates; they exhibited satisfactory performance without any signs of failure either in the form of debonding or fracture. This is shown by the bending moment versus mid-span deflection curve plotted for this test in figure 8. Despite the satisfactory performance of the CFRP laminates, no increase in the flexural bending capacity could be achieved due to the slab damage from its previous loading history; however; the performance of the anchors for the attachment of the CFRP laminates was satisfactory and the flexural behavior of the slab exhibited a much larger range of deformability (figure 8).

2.2. Upgrading the flexural and shear capacity of beams

The upgrading of the shear / flexural capacity will be presented in this section together with the corresponding modes of failure of reinforced concrete (R/C) beam specimens including repair schemes with Fibre Reinforcing Plastics (FRP) ([13], [25], [26], [27], [14], [28], [29]). The specimens were constructed and tested at the laboratory of Strength of Materials and Structures of Aristotle University. The applied load and the deflections of the specimen at three points were monitored throughout the experiments. Moreover, strain gauges were applied at selective locations of the FRP strips employed in the repaired specimens in order to monitor their state of stress during the loading sequence. In what follows, the most important experimental results are presented together with a discussion of the observed performance in order to highlight the role of the FRP strips in the observed behavior. It must be stressed that in all the studied beam specimens closed loop FRP hoops could be applied; this cannot be done in T-beam sections [19].

2.2.1. The initial reinforced concrete beam specimen and its observed behavior.

The virgin beam specimen: The virgin specimen BEAM-1 is a typical R/C beam, shown in figure 10, of rectangular cross-section of 200 mm x 500 mm and length l = 3700mm, having longitudinal reinforcement 3Φ20 at the top and 3Φ20 at the bottom side with closed stirrups as transverse reinforcement Φ8/250 ([14]). The selected longitudinal and transverse reinforcement together with the loading arrangement, shown in figure 11, will lead

http://dx.doi.org/10.5772/51326

the behavior of this virgin specimen to be dominated by the shear rather than the flexural mode of failure.

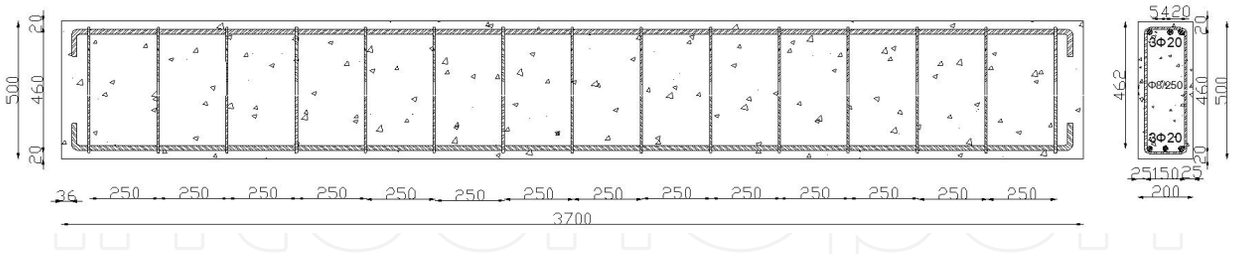

Figure 10. Dimensions (in mm) and structural details of specimen *Beam-1*. Longitudinal reinforcement: 3Φ20 at the top and 3Φ20 at the bottom. Transverse reinforcement: Φ8/250.

The behavior of BEAM-1: The specimen was simply supported at two point supports and was subjected to loads at two points symmetrically spaced at a distance 1150mm from each support; the mid-part had a length of 700mm. This loading was gradually increased, being monitored all the time. Moreover, throughout the loading sequence till the failure of the specimen, the cracking pattern was monitored together with the deflections of the beam at three points (mid-span and under each point load). As can be seen in figure 11, the shear cracking pattern is predominant at the two sides of the beam, whereas the middle part, as expected, is dominated by the flexural behavior. Finally, the dominant failure mode was from shear, as was planned during the design of this specimen. Figure 12a depicts the observed shear cracking patterns. In order to facilitate the repair of this specimen the loading was stopped after a decrease in the bearing capacity of the specimen was observed. In this way, the permanent deformations of this specimen at this stage were rather limited and the shear mode of failure was not allowed to fully develop.

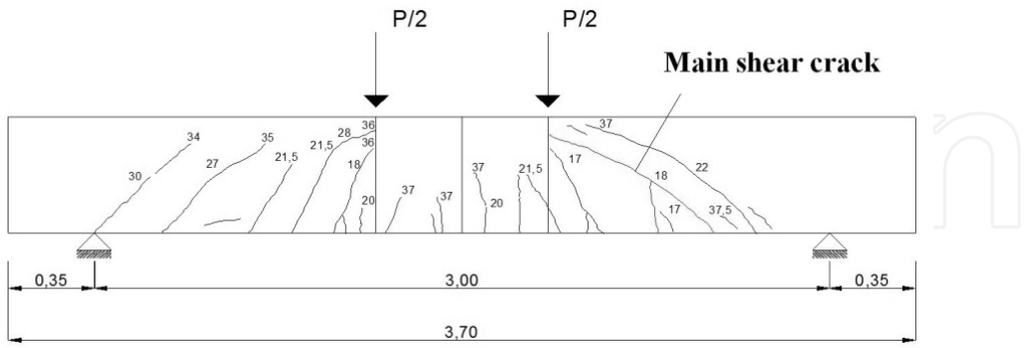

Figure 11. Flexural and shear cracking patterns for specimen *Beam-1*. Prevailing final mode of failure the shear.

Evaluation of the observed behavior for specimen BEAM-1: Figure 12b depicts the observed behavior in terms of shear force (Q). In the same figure the horizontal lines of different colours indicate the shear capacity of this particular specimen, as was predicted following the procedure suggested by various researchers ([30], [31], [32]) as well as by ei-

ther the Greek Code [9] (without safety factor) or by the Euro-code [7] (with safety factor). Figure 12c depicts the observed behavior in terms of bending moment (M). Again, the horizontal lines of different colours in this figure indicate the flexural capacity of this specimen as predicted by well established formulae as well as by the corresponding code procedures (without safety factor). Bearing in mind that the mode of failure is dominated by shear and not flexure the comparison between the shear and flexural limit states predicted in this way confirms the observed behavior.

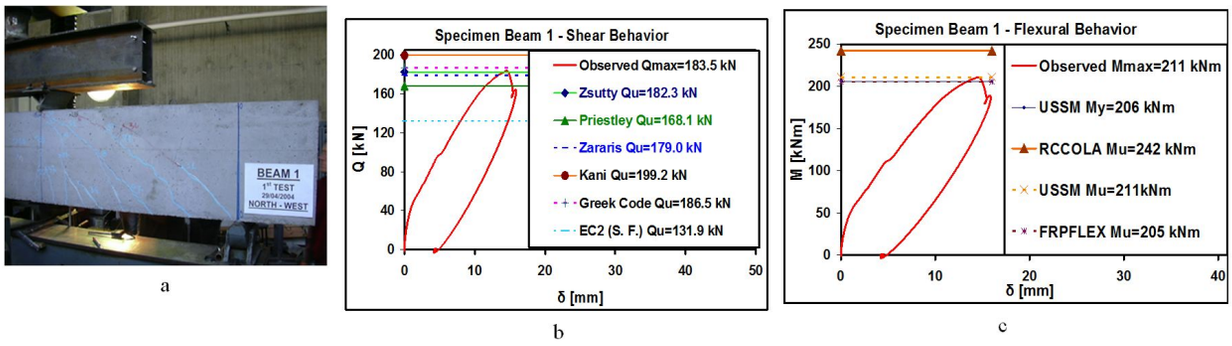

Figure 12. a Cracking patterns of Beam-1. b Evaluation of Shear Behavior (BEAM-1). c Evaluation of Flexural Behavior (BEAM-1).

2.2.2. Repaired beam specimen BEAM 1R-1 and observed behavior.

Description of Specimen BEAM 1R-1: After the end of the loading sequence of specimen BEAM-1, this specimen was repaired against shear failure in the way shown in figure 13. Closed loop CFRP (type C1 – 23) hoops of two layers (of nominal thickness 0.133mm per layer), having width b_{slice} = 75mm, were attached externally on the specimen spaced at distances of s=275mm. This was very easy to apply to this specimen and the only necessary treatment was to round up the corners of the specimen. However, in order to apply exactly such a repair scheme in prototype conditions one is faced with the considerable difficulty in drilling the appropriate holes at the top R/C slab that is usually monolithically connected to the beam at its top part. Moreover, the attachment of the CFRP layers in closed loop hoops will cause considerable difficulty. Alternatively, the CFRP shear reinforcement may not be of the closed loop hoop type but of the open loop U-shaped strips with or without anchors. The shear and flexural cracking that developed in specimen Beam-1 from the previous loading sequence was left without any repair (by epoxy resins or other means). An external layer of resin was used to paint the areas of the cracking in order to be able to monitor the activation of these cracks during the new loading sequence [14]. The mechanical properties of the employed CFRP layers (type C1 – 23), as they are given by the manufacturer, are : Ultimate stress f_u = 3800 Mpa, Young's Modulus E_f = 230 Gpa, Limit strain ε_u = 1.8 %, thickness t_f = 0.133 mm.

http://dx.doi.org/10.5772/51326

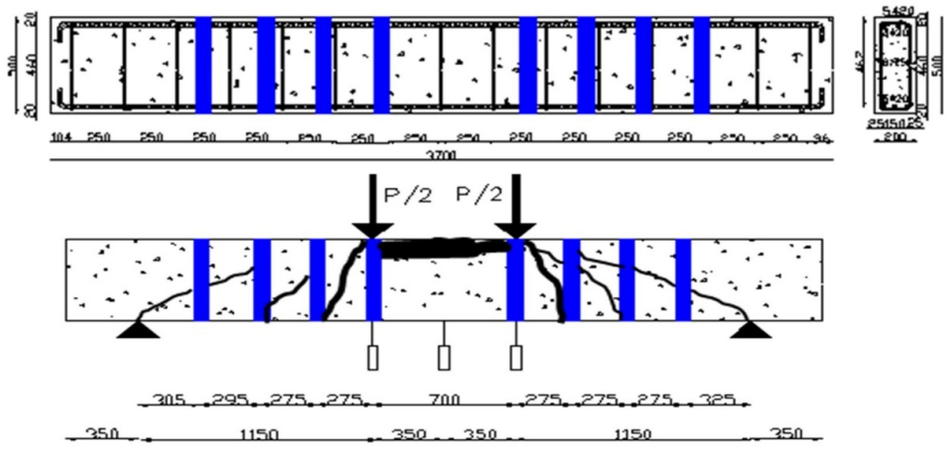

Figure 13. Repaired specimen BEAM 1R-1 The newly activated cracks are shown with bold lines. Dominant mode of failure the one at the compression zone of the mid-part of the specimen governed by flexure.

Observed Behavior of Specimen BEAM 1R-1: The main shear crack at the right side gave signs of becoming active for vertical load of 177KN (Q=88.5KN) whereas the same occurred for the left side main shear crack for vertical load of 216KN (Q=108KN). This meant that the corresponding CFRP shear type hoops started to develop stresses resisting part of the shear. Crushing was observed at the compressive upper side of the mid-part of this specimen undergoing flexure, when the vertical load reached 373KN. This was accompanied by the activation of the flexural cracks starting from the bottom side of the beam. These vertical flexural cracks developed even further for a maximum load of 414KN extending all the way from the bottom side to the crushed upper side, with the specimen reaching its flexural capacity. The shear mode of failure of the previous specimen was contained without further development by the applied CFRP hoops. The final condition of this specimen is depicted in figure 13. The observed behavior in terms of shear force (Q) and bending moment (M) is depicted in figures 14a and 14b. The maximum observed shear force was Q = 207 KN, and the maximum observed bending moment was M= 238 KNm.

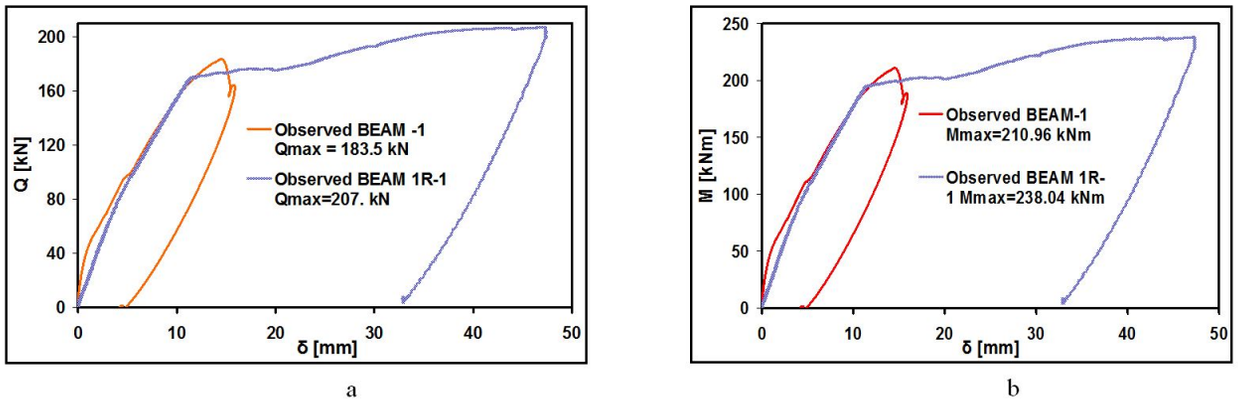

Figure 14. Observed shear behavior of BEAM 1R-1. 14b. Observed flexure of BEAM 1R-1.

In these figures 14a and 14b, the observed behavior before the repair of this specimen is also plotted for comparison with maximum observed shear force Q = 183.5 KN, and maximum observed bending moment M= 211 KNm. From this comparison it can be concluded that the applied CFRP hoops resisted a shear force of 23.5KN without signs of any distress. The successful increase (13%) in the shear bearing capacity of this specimen by this applied CFRP repair scheme, which leads to the exhausting of the specimen's flexural capacity and to reaching the desired flexural mode of failure, demonstrates the potential of such repair schemes for prototype conditions. However, there are construction difficulties in prototype conditions which were already pointed out before. Moreover, as was remarked before, the shear capacity of this scheme was not reached as the specimen survived the applied loading sequence in terms of shear. A subsequent reloading of specimen BEAM 1R - 1, with additional repair elements, namely specimen BEAM 2R -1, is presented in the following. The objective is to define by measurements the shear bearing capacity of the applied CFRP-hoops in this repair scheme.

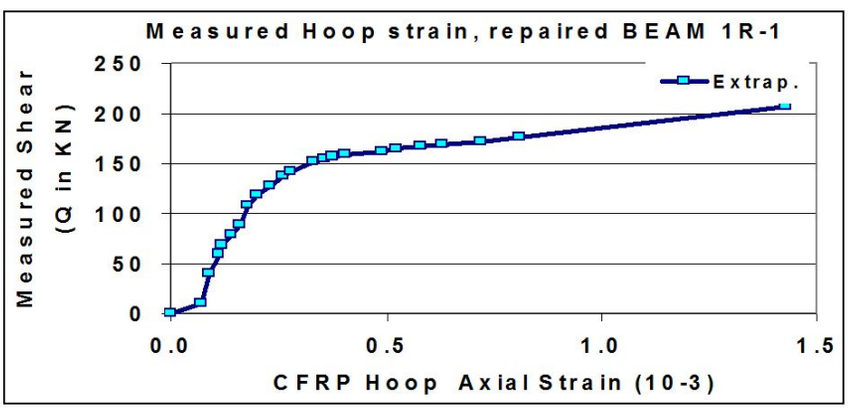

Figure 15. The variation of the CFRP-Hoop strain with the measured shear force for BEAM 1R-1.

Evaluation of the contribution of the CFRP for specimen BEAM 1R-1: During the loading sequence of Beam 1R-1, described above, the strains that developed at the mid-height of the third CFRP-hoop from the right end of the specimen (see figure 13) were monitored throughout the test by a strain gauge attached in this location. This strain gauge remained operational up to a total vertical load of 353KN (Q=177.6KN) measuring for this load an axial strain equal to 0.081 %. Unfortunately, beyond this load, the strain gauge became inactive due to a crack going through it. The variation of the axial (vertical) strain of CFRP-hoop with the applied shear force is depicted in figure 15. As can be seen in this figure, during the loading of specimen Beam 1R-1 the variation of the measured CFRP-hoop strain with the applied shear force is almost linear with different slope in two distinct ranges; the first range for shear force values up to Q=150KN and the second range for shear force values larger than Q=150KN. By extrapolating the second linear strain trend up to the maximum measured shear force value of 207KN a maximum strain value equal to 1.43 10^{-3} is found for the CFRP-hoop, which is also depicted in figure 15 (see also figure 14a). By employing the relationship: $V_f = A^{hoop}(h/s)E_f \varepsilon_f{}^{eff}$

http://dx.doi.org/10.5772/51326

where A^{hoop}=39.9mm2 the cross-section of one CFRP hoop, h=500mm the height of the beam, s=275mm the spacing of the hoops, E_f=230Gpa the Young modulus of the applied CFRP, ε_f^{eff} =1.43 10^{-3} the effective CFRP strain as was mentioned before, the value of the shear resisted by the applied CFRP-hoops can be found equal to V_f = 23.86KN.

When this value, which was found from direct strain measurements of the CFRP-hoop, is compared with the value of V_{fa} = 23.5KN, found by subtracting the shear resisted by the virgin specimen BEAM -1 from the shear resisted by the repaired specimen BEAM 1R-1 with the CFRP-hoops, a very good agreement is observed, which further validates the shear resisted by the applied CFRP-hoops. Using the software developed by Triantafillou [33] a prediction for the maximum shear force equal to 44KN is found to be resisted by the CFRP-hoop arrangement applied in BEAM 1R-1 (figure 13). The measured value of approximately 24KN and the observed shear performance of this specimen are in agreement with this predicted upper limit (44KN) for the CFRP-hoop shear resistance of the employed repaired scheme.

2.3. Repaired specimen Beam 1R-2

As described in section 2.2.2. before, a middle part compressive zone crushing was observed as a limit state for specimen BEAM 1R-1. After unloading this specimen the crushed concrete was removed and the whole area cleaned till the compressive longitudinal reinforcement became visible. The reshaping of the orthogonal form of this part of the beam was achieved with a paste from a mixture of cement and epoxy resin, which becomes hard in one day attaining a compressive strength of 30 MPa. The thickness of this layer of paste was 20mm above the compressive longitudinal reinforcement and the corners were given a smooth curvature. This upper zone was next reinforced with layers of CFRP (C 1-23), as shown in figure 16, in order to increase its compression capability through confinement. In addition, three layers of GFRP (G-60 AR) were attached at the bottom side of the specimen to enhance through tension its flexural capacity beyond the one provided by the existing longitudinal reinforcement (figure 16).

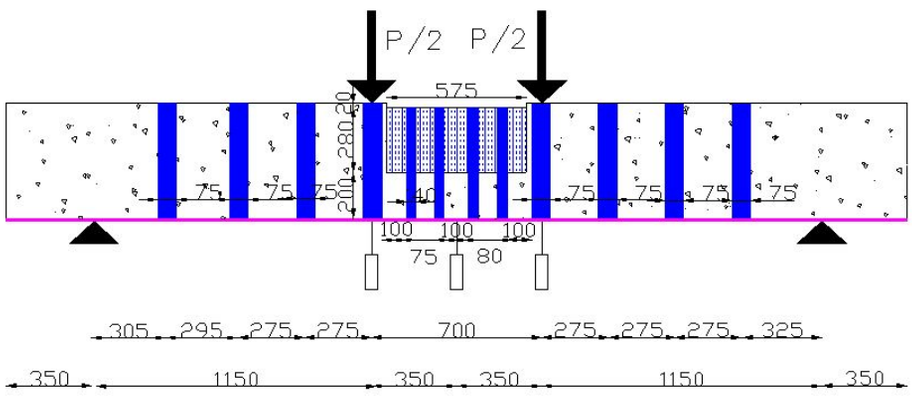

Figure 16. Specimen BEAM 1R-2 with CFRP layers attached in a way as to contain the compressive zone of the middle part as well as additional GFRP layer at the bottom side of the specimen extending the whole span.

2.3.1. Observed Behavior of Specimen BEAM 1R-2

This specimen was reloaded in a way similar to the one employed for the preceding specimens BEAM -1 and BEAM 1R-1. Figures 17a and 17b depict for all three specimens the shear and flexural behavior, respectively. In figure 17b the predictions of the yield moment for specimen BEAM-1 and the ultimate moment of specimen BEAM 2R-1 are also indicated. Due to an increase in the flexural capacity for specimen BEAM 2R-1 when compared to the preceding specimen BEAM 1R-1, resulting from the described repair scheme for specimen BEAM 2R-1, the shear failure mode prevailed this time. This mode of failure was accompanied by the rupture of the CFRP hoops as well as by crushing of the concrete at the compressive shear transfer zone neighboring the point of loading (figure 18). As expected, this specimen (BEAM 1R-2) exhibited an increase in its flexural capacity when this is compared with the flexural limit state attained during the preceding test of specimen (BEAM 1R-1). This fact demonstrates that the repair scheme described before, aimed to increase the flexural capacity of specimen BEAM 1R-2 proved to be successful. The observed maximum shear force during this test was $Q_{\alpha v}$ = 215.8KN whereas the maximum bending moment was $M_{\alpha v}$ = 248.2KNm. Comparing these values with the ones observed during testing the original virgin BEAM-1 it can be concluded that the applied repair scheme resulted in an increase of the order of 18% for the shear capacity and more than 18% for the flexural capacity; the exact increase in the flexural capacity could not be measured as the shear failure for BEAM 1R-2 prohibited this specimen from reaching its flexural limit state. The predicted flexural capacity of BEAM 2R-1 is listed in Table 1.

METHODOLOGY	MU [KN m]	Mode of failure
Ultimate stress strain method	**301.26**	Failure from compression of the top zone and of tension of the GFRP
FRPFLEX	**319.02**	Failure of compression zone

Table 1. Predictions of flexural capacity for BEAM 2R-1.

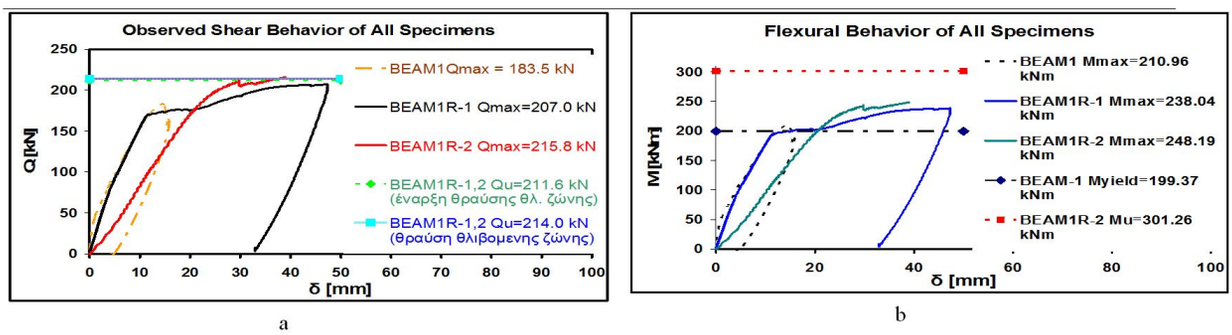

Figure 17. Shear behavior of all specimens. b. Flexural behavior of all specimens.

It must be pointed out here that the way the enhancement of the compressive zone capacity was achieved through the compressive zone confinement, attained from the CFRP layers,

http://dx.doi.org/10.5772/51326

cannot be applied so easily in prototype conditions due to the presence of an R/C slab at this part of a prototype beam. Table 2 lists the total vertical load values which were measured during important developments in the observed behavior of specimen BEAM 1R-2. Moreover, figure 19 depicts the observed mode of failure in a detailed way.

P [KN]	Description of the observed cracking
73.6	Partial activation of the shear cracks that were formed from past loading
166.8	Activation of the previously formed flexural cracks
235.4	Formation of main flexural crack next to the CFRP stirrup at loading point (left side)
343.4	Formation of main flexural crack next to the CFRP stirrup at loading point (right side)
421.8	Initiation of crushing of the concrete compressive zone at the shear transfer area neighboring the left loading point.
423.8	Rupture of a CFRP stirrup
431.6	Crushing of the concrete at the compressive shear transfer zone neighboring the left loading point. Rupture of the CFRP hoops that were crossed by the main shear crack (figure 18).

Table 2. Important developments in the behavior of specimen BEAM 1R-2 during loading.

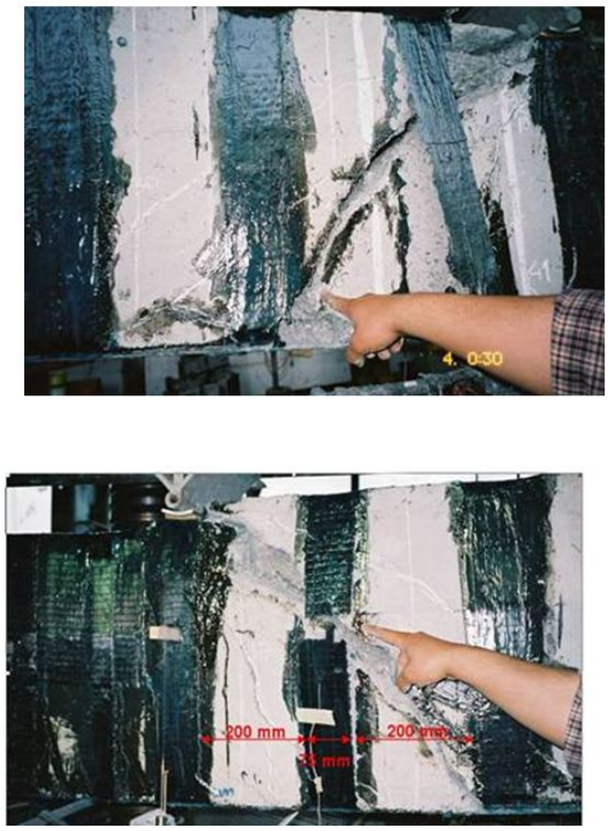

Figure 18. Shear failure accompanied by the rupture of the CFRP stirrups as well as of crushing of the concrete compressive zone at the shear transfer area neighboring the point of loading.

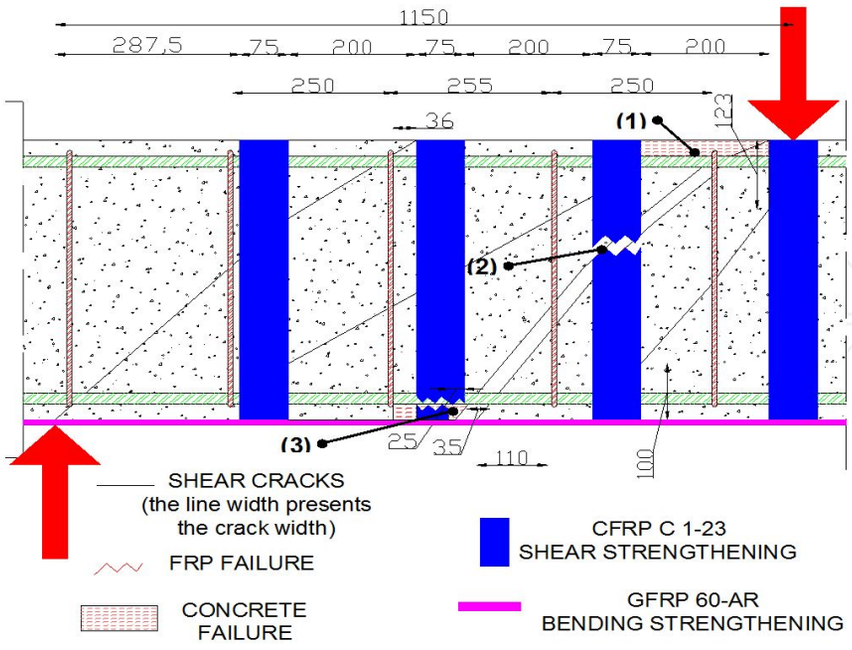

Figure 19. Mechanism of shear failure during the limit state of specimen BEAM 1R-2.

2.3.2. Evaluation of the contribution of the CFRP-hoops for BEAM 1R-2

As was done for specimen BEAM 1R-1, during the loading sequence of Beam 2R-1 the axial (vertical) strains that developed at the mid-height of the third CFRP hoop from the right end of the specimen (see figure 13) were again monitored employing a strain gauge attached in this location. This strain gauge remained operational throughout the whole load sequence measuring a maximum axial strain value $\varepsilon_f^{\ eff} = 0.67$ % when the total vertical load reached its maximum value of 435.6KN (Q=215.8KN). By subtracting the shear resisted by the virgin specimen BEAM -1 (Q=183.5KN) from the shear resisted by the repaired specimen BEAM 2R-1 (Q=215.8KN), a value of $V_{fa} = 32.3$KN is found as being resisted by the used repair scheme. As mentioned before, using the software developed by Triantafillou [33] the maximum shear force of 44KN is found to be resisted by the CFRP hoop arrangement applied in BEAM 2R-1. Moreover, employing the maximum strain measurement and the relationship $V_f = A^{hoop} (h/s) E_f \varepsilon_f^{eff}$ the shear resisted by the applied CFRP-hoops can be found equal to $V_f = 111.8KN$. This discrepancy dictates further investigation on the shear resisting mechanisms that developed during the limit state of specimen BEAM 2R-1 (see figure 19).

The maximum axial strain measurement equal to 0.67 % was recorded at this particular CFRP-hoop location during maximum applied load just before the rupture of this CFRP-hoop and the final development of the shear failure for specimen BEAM 2R-1. The variation of the applied shear force with the measured CFRP hoop strain is depicted in figure 20; it is almost linear with different slope in two distinct ranges; the first for a shear force value from zero to Q=205KN and the second for a shear force value larger than Q=205KN up to $Q_{\alpha v}$ = 215.8KN, when the rupture of the CFRP occurred.

http://dx.doi.org/10.5772/51326

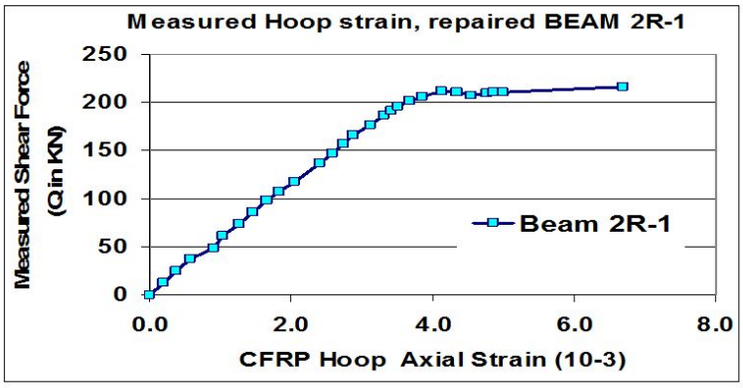

Figure 20. The variation of the CFRP-hoop strain with the measured shear force for BEAM 2R-1.

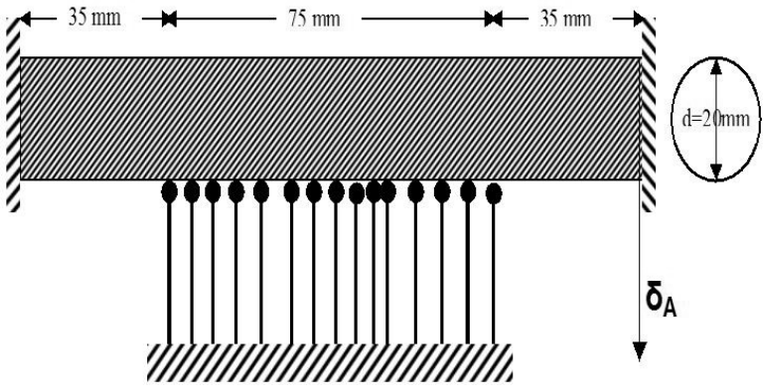

Figure 21. Numerical simulation of the dowel action.

2.3.3. Shear capacity of specimen BEAM 2R-1 based on the observed failure mechanism

Based on the observed shear failure mechanism, which is depicted in figure 19, the shear capacity of BEAM 2R-1 will be estimated as will be described below. It is assumed that the shear is resisted in this case by the following parts.

One closed steel stirrup.

The compressive zone for shear transfer next to the point of load application at the top of the main shear crack.

Two CFRP-hoops.

The contribution of the bottom side longitudinal reinforcement (dowel action).

The contribution of the compressive zone is found from the relationship: $V_c = 0.3\ (fc)^{2/3}\ (2)^{1/2}$ x b. Where fc the concrete compressive strength, x the height of the compressive zone (as estimated from the flexural behavior), b the width of the beam. This leads to a shear force equal to $V_c = 46.42$ kN at the initiation of concrete compressive zone crushing.

The contribution of the assumed two CFRP-hoops is equal to $V_f = 18234\ \varepsilon_f^{\ eff}$ [KN]. According to the strain measurements this contribution at the initiation of crushing of the compressive zone is equal to $V_f = 73.54$KN.

The contribution of the dowel action of the longitudinal reinforcement will be based on the geometry of this particular failure mechanism which was measured in detail at the laboratory. For this purpose, a simple numerical simulation of this dowel action was formed, which is depicted in figure 21. The longitudinal reinforcement is supported by a steel stirrup (left support) and by the CFRP-hoop (multiple mid-supports). All the supports are simulated by springs with the corresponding elastic / post-elastic and cross-sectional properties the actual steel stirrup and CFRP-hoop possess.

Due to the volume of concrete the rotations at the two ends of this dowel action numerical model were restrained; moreover, the employed simulation provided the capability for the longitudinal reinforcement to develop plastic hinges with parameters based on the cross-sectional area and yield stress of the employed longitudinal reinforcement, which were measured at the laboratory.

The limit state contribution of the dowel action of the longitudinal reinforcement, as resulted from this numerical simulation, was found equal to $V_d = 37.67$ KN. The contribution of the steel stirrup (V_w) is based on the assumption that its strain is the same as the measured strain of the neighboring CFRP hoop. The various contributions based on all the above assumptions are listed in Table 3 together with the corresponding total measured value. As can be seen a very good comparison is reached between the total estimated shear resistance and the corresponding measured value. It must be pointed out that the estimated value was based on the exact observation of the failure mechanism as well as on the measurements of the CFRP hoop strains. In the same table a predicted shear resistance value is also listed based on the prediction of the maximum shear resisted by the CFRP-hoops by the software developed by Triantafillou [33] (maximum predicted V_f value equal to 44KN is found).

Steel Stirrup V_w [KN]	2 CFRP Hoops V_f [KN]	Dowel action of longitudinal reinforcement (3Φ20) V_d [KN]	Compressive Zone of Concrete V_c [KN]	Total estimated shear resistance V_R [KN]
53.94	**73.54**	**37.67**	**46.42**	**211.57**
Measured total shear resistance **210.9KN**			Predicted total shear **227.5KN** [ref. 33]	

Table 3. Shear resistance contributions of the various parts of specimen BEAM 2R-1 at the initiation of the compressive zone crushing.

The variation of the estimated shear contributions of the CFRP-hoops (Vf), the steel stirrup (Vw), the dowel action of the longitudinal reinforcement (Vd) as well as the sum of all these (Vf+Vw+Vd) are plotted in figure 22 together with the measured total shear force (V_R) for specimen BEAM 2R-1. The common basis for the plotted displacements between the estimated contributions and the measured values is found from the correspondence of the load and strain measurements during testing. In addition, in the same figure, the variation of the

http://dx.doi.org/10.5772/51326

contribution of the compressive concrete zone is plotted by subtracting from the total measured shear force (V_R) the contributions of the steel stirrups and the CFRP hoops ($Vc=V_R-Vw-Vf$). After the formation of the shear cracks this contribution includes the dowel action of the longitudinal reinforcement. This results in a maximum value Vc = 84.14 KN, which is in agreement with predictions based on formulas suggested by various researchers. Moreover, it can be seen that the summation of the various contributions is in good agreement with the total measured shear force if the contribution of the compressive zone is added, after the formation of the shear cracks and up to the initiation of the crushing of the compressive zone concrete.

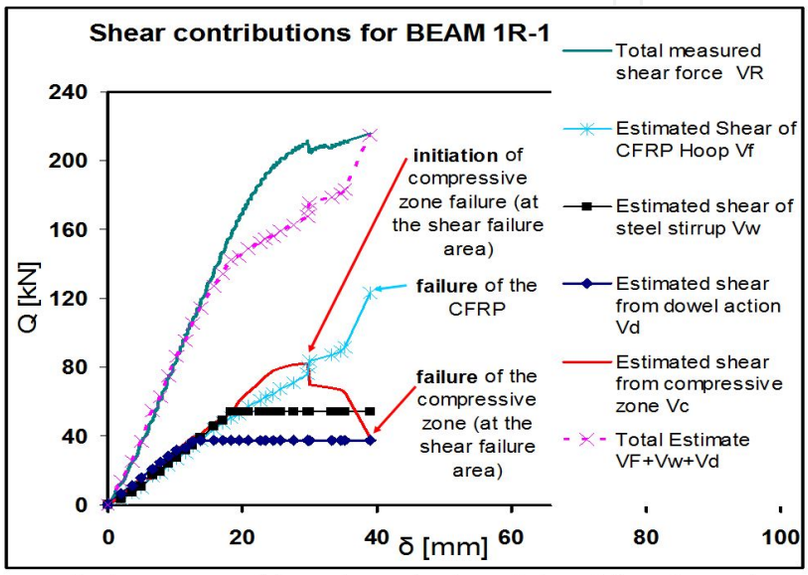

Figure 22. Shear resistance contributions, extracted from the mechanism of shear failure for specimen BEAM 2R-1.

2.4. Concluding observations

a1. The technique of repairing reinforced concrete beam elements by attaching CFRP layers has been examined in the laboratory. It was found that using CFRP-hoops, spaced at the areas of the beam that resist the shear forces, was a quite successful repair technique in upgrading the shear capacity of beam specimens by inhibiting the shear mode of failure thus favouring the development of the flexural mode of failure.

b1. The repairing of the examined specimens by attaching GFRP layers to complement the tensile longitudinal reinforcement together with CFRP confinement of the compressive zone at these parts of the beam that undergo flexure was again a quite successful technique in upgrading the flexural capacity of the beam specimens. However, this must be properly controlled in order to prohibit the development of the undesired shear mode of failure.

c1. In order to be able to successfully control the shear and flexural capacities and modes of failure, after the application of CFRP repair schemes, reliable tools are necessary that successfully predict the bearing capacities of the repaired structural elements. It was demon-

strated by this work that whereas this is possible for the flexural capacity it is not so straightforward for the shear capacity unless the basis of the shear capacity estimate is founded on a realistic failure mechanism that takes into account the realistic contributions of all the parts that are mobilized through this failure mechanism.

d1. It must be pointed out that the examined repair schemes for upgrading the shear resistance through CFRP stirrups will not be so easily applied in prototype conditions where the presence of a reinforced concrete slab, cast monolithically with the upper part of the beam, must be confronted.

Figure 23. R/C cross-sections with one side longer than the other (h/b>1.5) and CFRP partial confinement.

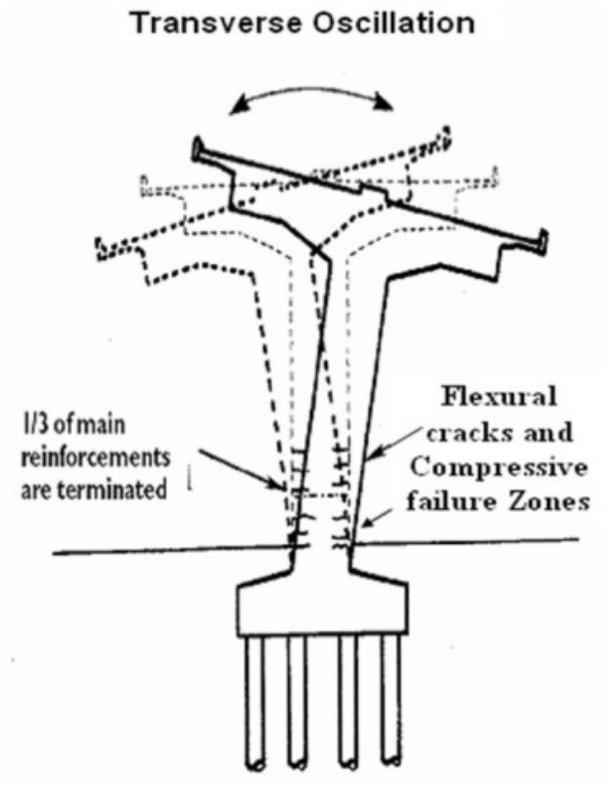

Figure 24. Bridge Pier compression failure mode.

http://dx.doi.org/10.5772/51326

3. Partial Confinement

3.1. The use of confinement for upgrading the flexural and shear capacity of columns.

A very common application of externally applied fiber reinforced plastics (FRP) is confining parts of structural members. This can be easily envisaged for columns with their cross-section approximating a square shape [34]. This is done by wrapping around the structural element one or more that one layers of FRP sheets together with the proper resine in-order to bond them on the surface of the structural member as well as to bond the FRP sheets between themselves. The main points of attention here are the following [35]:

Preparation of the surface of the existing structural member in order to prohibit premature delamination (debonding) of the attached FRP sheets.

Localized rupture of the FRP jacket due to abrupt change of curvature at the corners, to buckling of reinforcing bars, or to excessive dilation of concrete.

Proper application of the resin in order to achieve sufficient bond between the FRP sheets and the surface of the existing structural member.

Proper application of the resin and enough overlapping length of the wrapped layers of the FRP sheet around the existing member in order to prohibit any unwrapping mode of failure.

The proper wrapping of the FRP multilayer sheet around the existing structural member (column or beam) introduces a passive confinement in the same way as steel stirrups do on such concrete members. Whereas the wrapping of FRP sheets around columns or beams of rectangular shape with width / height ratio no greater than 2 can be easily materialized this is not so easily applicable in the following cases:

In columns with rectangular cross-sections having a width / height ratio greater than 2. It will be discussed later on in this section how this difficulty was confronted in the laboratory.

In T- beams whereby the presence of the slab prohibits the wrapping of the FRP sheets around the cross-section.

Grade	Compression failure mode	Increase in the compressive capacity (compared to the unconfined specimens)	Effectiveness of the partial confinement
1	Of the weak part as without the partial confinement	Small increase	**low**
2	Of the weak part as without the partial confinement	Considerable increase	**Considerable**
3	Of both the weak part and the strong parts	Substantial increase	**Very effective**

Table 4. Characterization of the effectiveness of the partial confinement.

The beneficial effect of such a confinement on the compressive strength of axially loaded structural members is well known and will not be repeated here. Moreover, the function of these externally applied FRP sheets as transverse reinforcement for both columns and beams is also evident in the same way closed steel stirrups function in reinforced concrete sections. Acting as external transverse reinforcement FRP sheets fully wrapped around beams or columns can be utilized to upgrade their shear capacity (figure 5). This has been already discussed in the beginning of section 2. Again, for T-beams the presence of the slab prohibits the formation of closed loop transverse reinforcement by the FRP sheets. If the FRP sheets are applied as transverse reinforcement in an open loop formation they are susceptible to a premature delamination type of failure (see figure 4). This will be further discussed in section 6 together with the way this difficulty was confronted in the laboratory.

The upgrading of reinforced concrete (R/C) cross-sections, with one side rather longer than the other (h/b > 1.5), by partial application of CFRP (Carbon Fiber Reinforcing Plastic) confinement is investigated here (figure 23). This partial application of CFRP confinement is aimed at the retrofitting of bridge-pier type R/C cross-sections in order to prohibit, up to a point, the development of premature compressive failure at the base of the pier due to combined compression and flexure from seismic loads (see figure 24 and [36], [37]). The performance of such structural elements was studied extensively in the past ([38], [39]). This type of partial confinement may also be applied to upgrading vertical structural members with non-accessible sides. Design guidelines for rectangular FRP jackets applied on rectangular columns have been proposed with the limitation that the cross-sections have aspect ratio h/b < 1.5 [37]. For higher aspect ratios it is recommended to design a circular or oval jacket. However, it is expected that for rectangular cross sections with aspect ratios larger than 1.5 the radius of a circular or rectangular jacket will be too large and will result in ineffectual confinement and will prove costly and impractical. For this reason it is desirable to investigate alternative schemes for increasing the confinement of rectangular cross-sections with relatively large aspect ratio without resorting to complete circular or oval jackets. Such a scheme is studied here using CFRP layers that do not extend all around the cross-section (figure 23 "*partial confinement*").

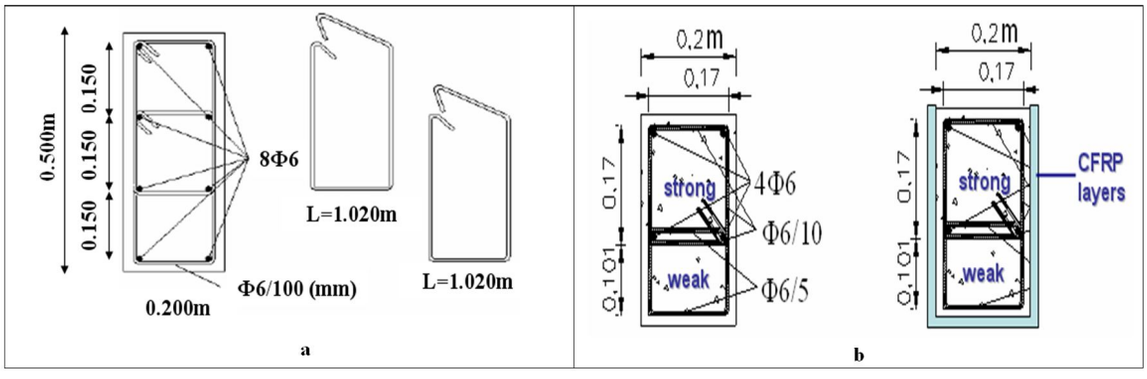

Figure 25. Initial cross-section with h/b ratio = 2.5. 25b. Test specimens without and with partial CFRP confinement.

http://dx.doi.org/10.5772/51326

To compensate for the fact that the CFRP layers do not enclose the cross-section entirely, anchorage of these layers must be provided, as shown schematically in figure 23. To this end, a laboratory investigation was carried out to study the effectiveness of such partial confinement together with alternative anchorage schemes. As will be explained, this effectiveness was tested by subjecting the specimens only to compressive loads. Despite this limitation, as will be demonstrated from the results of this investigation, the most significant aspects of the critical factors for this "*partial confinement*" scheme were brought to light.

3.1.1. The formation of test specimens

The initial cross-section, which formed the basis of the tested specimens, is depicted in figure 25a with an aspect ratio h/b equal to 2.5. This is a rectangular cross section of a bridge pier model structure, which was tested both at the laboratory (figure 25a) and at the Volvi-Greece European Test Site in the framework of the European project Euro-Risk [36]. This cross section was intentionally designed to develop flexural mode of failure at the base of the pier; moreover, it was desirable to find ways to retrofit such specimens by prohibiting premature compression failure at the base by means of partial CFRP confinement. The effectiveness of the partial CFRP confinement is studied by subjecting the tested specimens only to pure compressive loads. This type of stress field is expected to develop at the base of such vertical members under combined vertical loads and seismic actions, where undesired compression failure may develop. In order to limit the maximum level of compressive loads required to bring to failure such a cross-section with the loading arrangements available, the tested specimens had a cross section (figure 25b) of 200mm by 300mm instead of 200mm by 500mm of the initial cross-section (figure 25a and figure 25b) for the bridge pier specimens tested both at the laboratory and at the test site under combined compression and flexure [36]. Moreover, in order for the tested specimens to form compression failure at the same part of the cross-section where such failure would develop at the base of the initial bridge pier model, one part of the tested cross-section was left identical to the initial cross-section (the one that is marked in figure 25b as weak) whereas the remaining part was strengthened both with longitudinal and, in particular, with transverse reinforcement (the one marked in figure 25b as strong).

In this way, with the compression capacity of the weak part being smaller than that of the strong part, the compression failure was expected to develop at the weak part. This proved to be correct during the experiments, as will be shown in the following sections. The CFRP partial confinement was applied at the weak part, as is shown at the right hand side of figure 25b. Then, by studying the resulting bearing capacity and mode of failure under compression of the tested specimens (with or without partial confinement) the effectiveness of such a repair scheme could be demonstrated and classified as listed in table 4.

3.1.2. Construction of test specimens

Ten identical specimens were constructed and eight of them were used in the current experimental sequence (see table 5). All specimens were reinforced in the same way and were cast at the same time with the same mixture aiming for similar plain concrete strength values.

The reinforcing details are depicted in figure 26. As can be seen, the total height of the specimens was 1600mm. They had a mid-part height of 580mm that was left to develop the compression failure (figure 26, part denoted as CROSS SECTION A). The cross section of this mid-part was the one shown in figure 25b, including the two distinct parts (the weak and the strong). The two edges of the specimens, with a height of 510mm each, were confined during the experiment with strong steel brackets covering these parts from all sides thus prohibiting any compressive failure developing at those two edges (see figure 27).

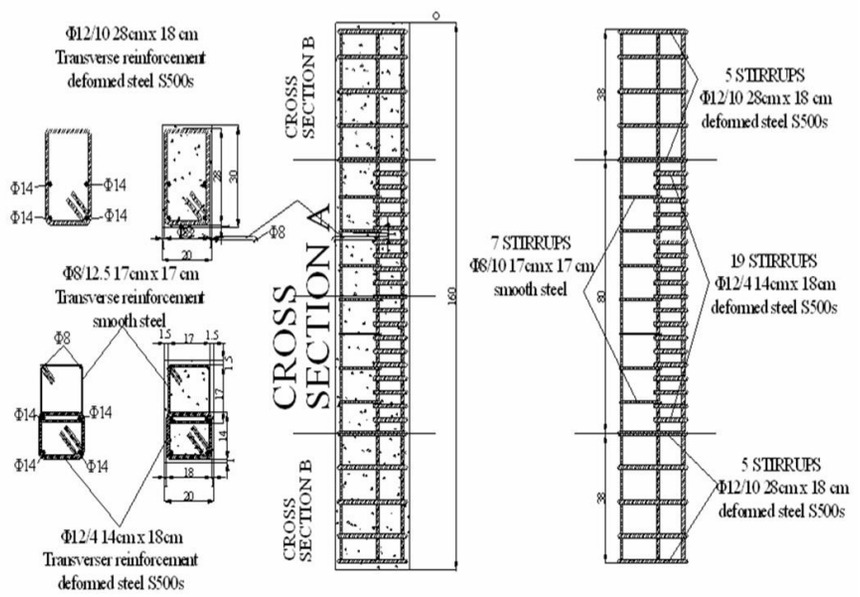

Figure 26. Reinforcement details common to all specimens.

Virgin Specimens	CFRP Confinement	Repaired Specimens	Plain Concrete Strength (Mpa)
Specimen 1 Test 1	No	Test 2 3+(2) CFRP	28.0
Specimen 1a Test 1	3 CFRP layers	Test 2 3 GFRP	25.8
Specimen 3 Test 1	No	Test 2 3+(2) CFRP	27.6
Specimen 3a Test 1	5 CFRP layers	Test 2 5 CFRP	27.6
Specimen 4 Test 1	5 CFRP layers		27.7
Specimen 4a Test 1	5 CFRP layers		27.7
Specimen 5 Test 1	5+(2) CFRP layers	Test 2, 5+2 CFRP Test 3, 5+2 CFRP Test 4 7 CFRP	27.6
Specimen 5a Test 1	No	Test 2, 7 CFRP Test 3 7+4 CFRP	25.8

Table 5. Test specimens with their corresponding concrete strength.

http://dx.doi.org/10.5772/51326

The partial CFRP confinement was attached only on the three sides of these specimens covering the weak part and leaving the fourth side (of the strong part) free without any CFRP layers (figure 25b). There were 8 virgin specimens, namely 1, 1a, 3, 3a, 4, 4a, 5, and 5a (Table 5). These specimens were tested in their virgin state in which some of them were without partial CFRP confinement whereas the rest had the partial CFRP confinement applied to them from the beginning. The second column of table 5 indicates the partial confinement condition of the virgin specimens. The testing sequence of these virgin specimens is signified as Test 1. Most of these specimens were repaired after they had reached their limit state during their previous test. In all the repaired specimens the CFRP partial confinement was applied. Throughout these series of experiments the nominal thickness of the employed CFRP layers was 0.176mm with a given Young's Modulus E=350GPa. The measured maximum axial CFRP strain was approximately 1%.

Figure 27. Specimen with confining steel brackets at the edges and partial CFRP confinement at the mid-part

This sequential test number of the repaired specimens is signified as Test 2 (for the 1st repair), Test 3 (for the 2nd repair) etc. (see column 3 of Table 5). In the same column the number of CFRP layers used in the partial confinement for the repaired specimens is also indicated. The total number of specimens, virgin and repaired, was seventeen. In Table 5 the unconfined concrete compressive stress is also listed, found from cylinders with diameter 150mm and 300mm height; these cylinders were obtained during the casting of each virgin specimen. The anchorage of the CFRP layers was applied along the two long sides, which were common to both the weak and the strong parts. The main load that was applied was axial compression, although in limited specimens the axial compression was combined with bending, which is not reported here. From the observed behavior, the effectiveness of the applied partial confinement could be deduced. As shown in table 4, this judgment was based on the level of the bearing capacity combined with the type of compression failure that was formed (at the weak or strong part). Moreover, the observed behavior of the various parts of the test specimens, such as the CFRP layers and their anchorage, helped to identify the factors that bear an adverse or beneficial influence on these aspects of the behavior.

3.1.3. Critical parameters and their variation:

The following parameters were critical (see results contained in Table 6).

1 st . The type of anchorage of the CFRP layers, 2 nd . The number of the CFRP layers.

The second parameter becomes critical only if the first parameter performs satisfactorily. A large number of specimens (1, 1a, 3, 3a, 4 and 4a) exhibited failure of the anchorage of the partial confinement thus limiting the effectiveness of the partial confinement to low levels. Consequently, the increase in the compressive bearing capacity in this case was relatively modest. The compressive load was monitored by continuous sampling throughout the test. The "*Average Stress at failure*" listed in table 6 is found by dividing the compressive load by the gross cross-sectional area of each specimen. Listed in table 6 are certain particulars of the anchorage of the CFRP layers. Anchors-1 signifies bolts of 7mm diameter and 60mm length that do not penetrate the cross-section in its whole width, whereas Anchors-2 signifies bolts of 10mm diameter that penetrate the whole section (220mm length).For specimens 5 and 5a, due to the improvement of the anchoring details of the partial confinement, the increase in the compressive bearing capacity of these specimens was 50% higher than the observed bearing capacity of similar specimens with no partial CFRP confinement. When the maximum compressive bearing capacity achieved with the partial confinement is compared with the corresponding plain concrete strength value, a 230% increase can be observed. Moreover, the compressive failure in this case involved both the weak and the strong part thus improving substantially the effectiveness of the partial confinement and allowing the employment of a large number of CFRP layers.

http://dx.doi.org/10.5772/51326

Specimen No	Virgin	Repaired	Number of CFRP layers	Anchors-1	Anchors-2 + washers	Average Stress at failure (Mpa)	Failure Mode
1 Test 1	Yes	No	No	No	No	41.12 (146.9%)*	Weak part
1 Test 2	No	Yes/ EMACO	3 (+2)	Yes	yes	41.69 (148.9%)	Bolts
1a Test 1	Yes	No	3	Yes		45.78 (177.4%)	Pull out Anchors-1
3 Test 1	Yes	No	No	No		40.79 (147.7%)	Weak part
3 Test 2	No	Yes	3 (+2)	Yes	Yes	45.78 (165.9%)	anchorage
3a Test 1	Yes	No	5	Yes	Yes	47.09 (170.6%)	anchorage
3a Test 2	No	Yes/ EMACO	5	Yes	Yes	42.51 (154.0%)	anchorage
4 Test 1	Yes	No	5	No	Yes weak	46.60 (168.2%)	anchorage
4a Test 1	Yes	No	5	No	Yes weak	45.53 (164.4%)	anchorage
5 Test 1	Yes	No	5 (+2)	No	Yes strong	53.96 (195.5%)	Steel bracket
5 Test 2	Yes	-	5 (+2)	No	Yes strong	55.26 (200.2%)	Steel bracket
5 Test 3	-	Top / EMAKO	5 (+2)	No	Yes Strong	53.96 (195.5%)	CFRP mid-height
5 Test 4	No	Yes/ EMAKO	7	No	Yes Strong	58.86 (213.3)	Strong stirrups
5a Test 1 bending	Yes	No	No	No	No	40.88 (158.4%)	Weak part
5a Test 2	No	Yes	7	No	Yes Strong	57.23 (221.8%)	CFRP mid-height
5a Test 3	No	Yes	7 +4	No	Yes Strong	60.17 (233.2%)	Strong part

Table 6. *Summary of test results together with the basic specimen characteristics.* As % of the corresponding plain concrete strength.*

3.1.4. Instrumentation to obtain the average stress-strain behavior

Apart from monitoring the compressive load, the deformations of the mid-part were also continuously recorded throughout each experiment with displacement measurements taken

at each side of the cross-section. Eight displacement sensors (two at each side) were employed to record the deformations of the mid-part. Although the deformation of this mid-part was far from uniform, as can be seen from the obtained displacement measurements of the weak and strong parts (figure 29), the average axial displacement, which was found by averaging the measured displacement values at all four sides of each specimen, is mostly used here as an indication of the deformability of each specimen. By dividing this average axial displacement by the height of the mid-part an average axial strain could also be obtained in this way. The following discussion of the observed behavior of each specimen is based on diagrams of average axial stress versus average axial strain found from the previously described averaging process. More detailed study on the obtained non-uniform deformability for each specimen will be carried out at a future stage. An additional measurement that was obtained during the experimental sequence was the axial strain that developed at the CFRP layers of the partial confinement of the mid-part. These CFRP strain measurements are an additional indication of the effectiveness of the partial confinement.

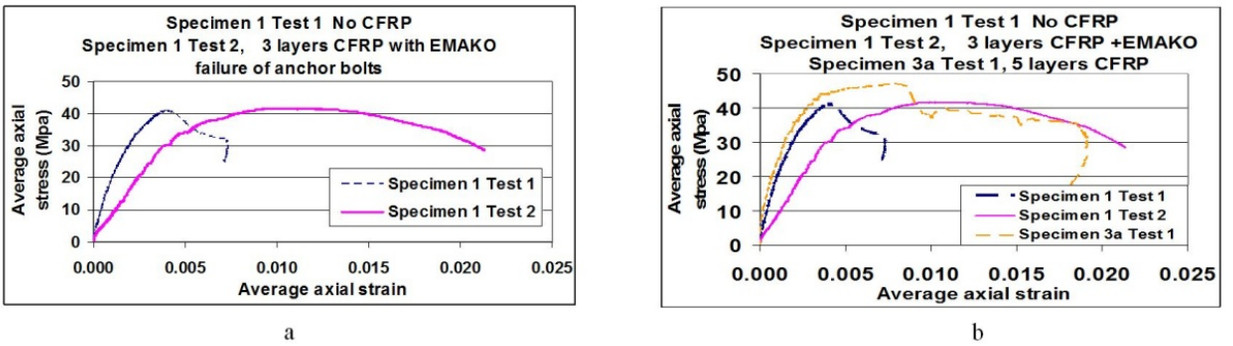

Figure 28. a Partial confinement of low effectiveness. b. Partial confinement of low effectiveness.

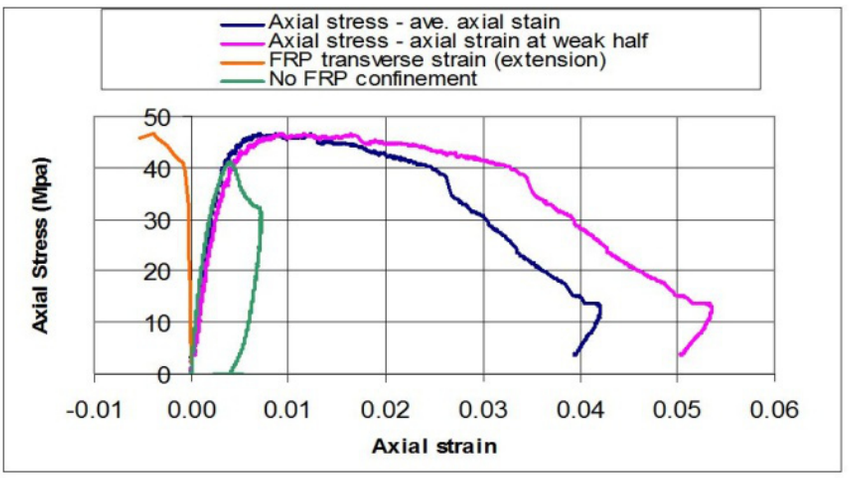

Figure 29. Specimen 4, Test 1 (5 layers CFRP) Comparison with Specimen 1 Test 1 (no confinement).

http://dx.doi.org/10.5772/51326

Figure 30. a Virgin Specimen without confinement. b. Failure of anchor bolts. 30c Low effectiveness of partial confinement. c. Tensile failure of CFRP Layers. Considerable effectiveness of partial confinement.

3.2. Discussion of the results

3.2.1. Partial confinement of low effectiveness

In figures 28a and 28b the obtained behavior of specimen1 (Test 2) with 3 CFRP layers and specimen 3a (Test 1) with 5 CFRP layers is compared with specimen 1 test 1 (no partial confinement). Specimen 1 test 2 was formed from specimen 1 test 1 by repairing the failed specimen 1 test 1 with special (low shrinkage) concrete as well as with 3 layers of CFRP forming the partial confinement. This repaired specimen failed in compression with almost the same capacity as the previously-tested virgin test with no partial confinement, but with larger deformability. The effectiveness of the partial confinement is low and it is due to the failure of the anchor bolts of the applied confinement. In figure 28b the observed behavior of specimen 3a Test 1 is also included. This is a virgin specimen that had a 5-CFRP layer partial confinement. Despite the increase in the CFRP layers, the observed effectiveness of the partial confinement is low as was for specimen 1 test 2, again because of the failure of the anchor bolts. In figure 29 the observed behavior of specimen 4 test 1 is depicted. This was a virgin specimen with 5 CFRP layers partial confinement. In this case, a certain alteration was applied in the anchor bolts, by increasing their length. However, this was not sufficient to improve accordingly the effectiveness of the partial confinement, which was again linked to the failure of the anchor bolts. The failed virgin specimen without the partial confinement is shown in figure 30a whereas figure 30b depicts the failure of the anchor bolts for the "low effectiveness" partial confinement.

3.2.2. Partial confinement of considerable effectiveness

In figures 31a and 31b the obtained behavior of specimen 5 (Test 3) with 5 (+2) CFRP layers is compared to specimen 1 test 1 (no partial confinement). Specimen 5 test 3 was formed by repairing a previously failed virgin specimen with special (low shrinkage) concrete as well as with 5 layers of CFRP forming the partial confinement. An additional two (+2) CFRP layers were applied at the part of the section where the anchor bolts were placed. This repaired specimen failed in compression with a modest increase (31%) in its capacity when compared with the capacity of the virgin unconfined specimen. The effectiveness of the partial confinement in this case was classified as considerable. This was due to an alteration in the anchoring of the partial confinement which proved to be relatively successful. The limit state for this specimen commenced with the tensile failure of the CFRP layers at the central zone and was accompanied, as expected, by a consequent compressive failure of the neighboring weak part of the section. This is depicted in figure 30c where the anchor bolts, which were left intact, are also shown. In figure 31b, the comparison is extended to include specimen 4 (Test 1), in which the partial confinement exhibited low effectiveness due to the failure of the anchor bolts.

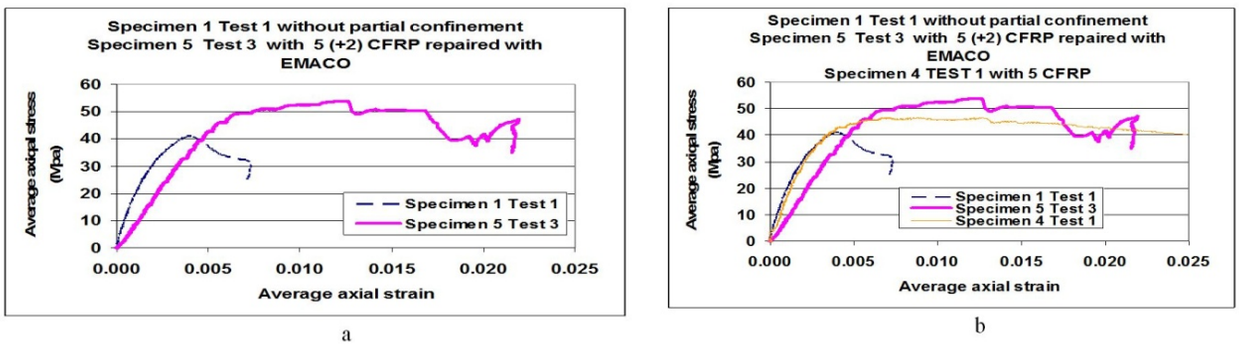

Figure 31. Partial confinement of considerable effectiveness. 31b. Partial confinement of considerable effectiveness.

3.2.3. Very effective partial confinement

In figure 32a, the behavior of specimens 5 (Test 4) and 5a (Test 2) is compared with the behavior of specimens 1 test 1 (with no partial confinement) and 5 (Test 3) discussed before. Specimens 5 (Test 4) and 5a (Test 2) were formed by repairing previously failed specimens with partial confinement of 7 layers of CFRP. Moreover, all the anchoring of their partial confinement was made with bolts going through the whole width of the strong part of the repaired section (see table 6 and figure 25). As can be seen in figure 32a, a substantial increase (40%), in the bearing capacity as well as in the deformability, resulted from the described partial confinement for these two specimens. Their behavior was in this way better than the behavior of specimen 4 (Test 1) which was classified before as one of considerable effectiveness of the partial confinement. Based in this increased capacity and deformability of specimens 5 (Test 4) and 5a (Test 2) they were classified as specimens with very effective partial confinement.

http://dx.doi.org/10.5772/51326

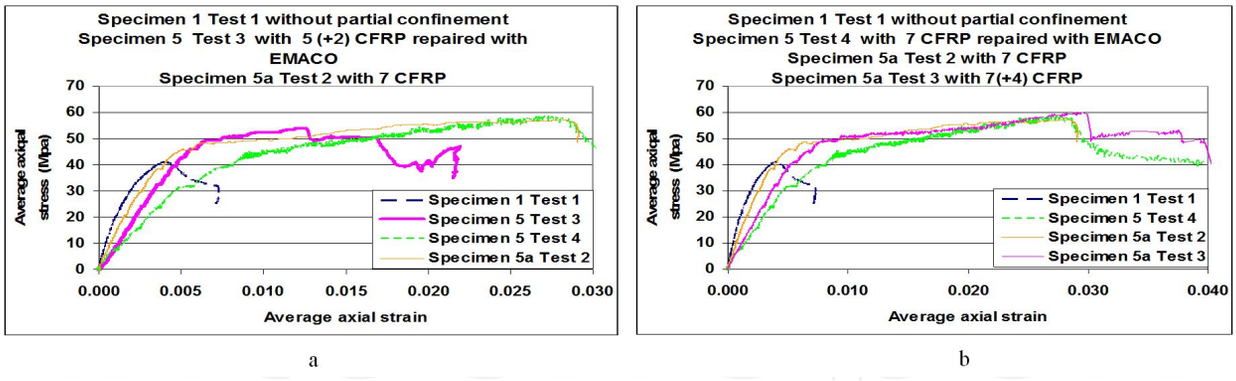

Figure 32. Very effective partial confinement. 32b. Very effective partial confinement.

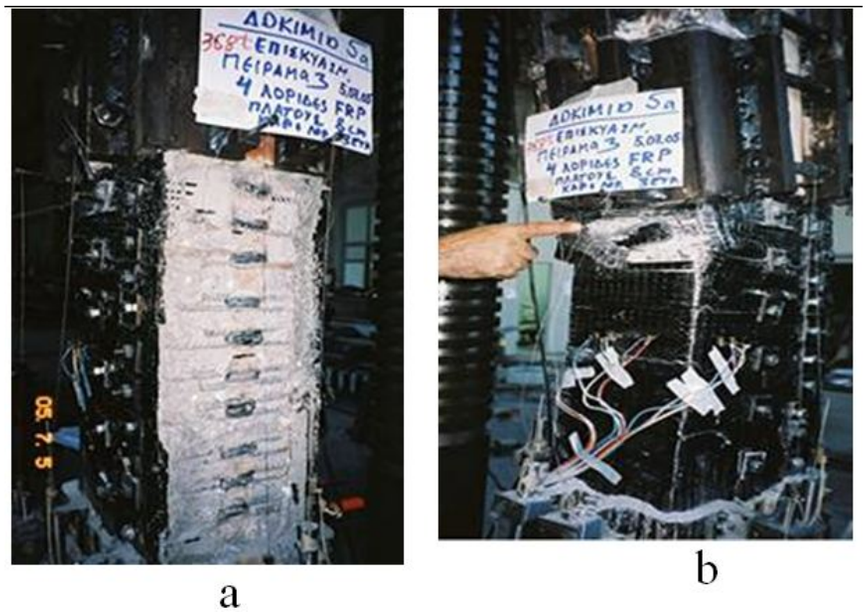

Figure 33. Strengthening stirrups - strong part. 33b. Failure of the CFRP layers of the mid-part.

The limit state of specimen 5 (Test 4) was accompanied with the failure of the stirrups of the strong part whereas the limit state of specimen 5a (Test 2) was accompanied with the tensile failure of the CFRP layers at the central zone. In figure 32b the observed behavior of specimen 5a (Test 3) is compared with that of specimens 5 (Test 4) and 5a (Test 2) previously discussed. Specimen 5a Test 3 had a partial confinement formed by 7 layers of CFRP. Moreover, the area sustaining the anchor bolts was strengthened by additional four (+4) layers of CFRP. Apart from the anchor bolts going through the whole width of the strong part of its section, the stirrups of this strong part were also strengthened (figure 33a). This time the increase in the bearing capacity was 46%; the increase in the deformability was also quite substantial. Thus, the behavior of this specimen is also one with very effective partial confinement. The observed limit state was accompanied with the compressive failure of the CFRP layers at the mid-part near the steel brackets (figure 33b).

3.3. Concluding remarks

a2. The undesired compression failure expected to develop in the base of vertical members with reinforced concrete cross sections having h/b ratio larger than 1.5 under combined vertical loads and seismic actions is studied through specially formed specimens subjected to uniform compression. The retrofitting of such specimens with partial CFRP confinement is aimed at prohibiting, up to a point, such compression failure. This type of partial confinement may also be applied to upgrading vertical structural members with non-accessible sides.

b2.. From the results of the experimental investigation with identical specimens, with or without this type of partial CFRP confinement, the successful application of such partial confinement was demonstrated. An increase of almost 50% was observed in the compression bearing capacity of some of the tested specimens. Moreover, the deformability of these specimens was substantially increased, demonstrating the effectiveness of this type of partial confinement.

c2. It was found from the experimental sequence that critical factors for this increase were the type of anchorage of the CFRP partial confinement and the number of CFRP layers. Successful anchoring of the CFRP layers allowed this partial confinement to become effective and to permit the use of a larger number of CFRP layers. In the present study alternative anchoring schemes were tried with limitations imposed by the geometry of the model cross-section. Similar limitations imposed by the geometry and the reinforcement of the cross-section will also dictate the design of such an anchoring scheme for a prototype cross-section. Further investigation on the performance of such prototype anchoring arrangements may be necessary.

4. Upgrading the flexural capacity of (R/C) vertical members

4.1. Flexural upgrading

The upgrading of the flexural capacity of reinforced concrete (R/C) vertical members with externally applied CFRP layers as means of tensile reinforcement is investigated here (see figure 34 and [4], [6], [11], [16], [22], [34], [40], [41])

The CFRP layers are applied at the two opposite sides of R/C specimens which were constructed for this purpose (figures 35a, 35b). They were designed with such longitudinal and transverse reinforcements shown in figure 35b that the flexural limit state would prevail. The specimens were tested to develop the ultimate flexural behavior with the corresponding damaged region concentrated near their joint with the foundation. These specimens had the foundation block fixed at the strong reaction frame of the laboratory of Strength of Materials and Structures of Aristotle University and were subjected to simultaneous constant vertical load as well as horizontal cyclic imposed displacements approximating thus the seismic actions. This loading sequence was applied prior to the application of any CFRP layers and was repeated again after these CFRP layers were attached to the damaged specimens. The observed upgrading of the flexural capacity in terms of ultimate overturning moment is presented and discussed.

http://dx.doi.org/10.5772/51326

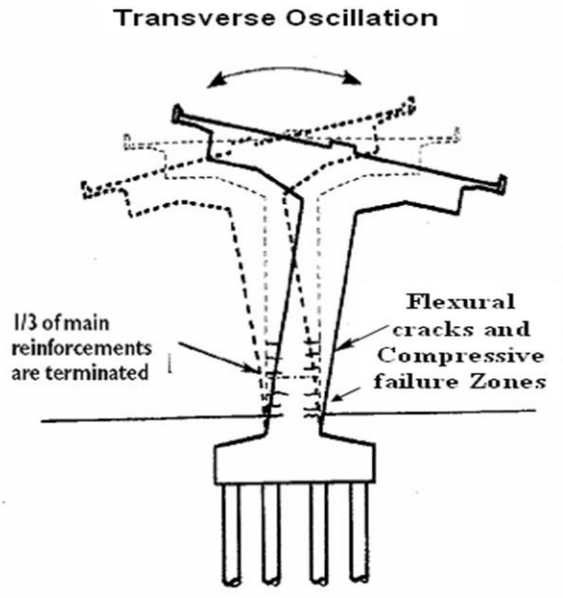

Figure 34. Flexural Damage

4.1.1. The virgin beam specimen

This specimen is shown in figure 35a with a rectangular cross-section of 200 mm x 500 mm and height h = 1815mm (from its top to the upper surface of its foundation). 8Φ6 was the longitudinal reinforcement that extended with no splices and was anchored to the foundation block and Φ6/100 closed stirrups the transverse reinforcement. The detailing of the cross-section is shown in figure 35b. The selected longitudinal and transverse reinforcement together with the loading arrangement, will cause the behavior of this virgin specimen to be dominated by the flexural rather than the shear mode of failure. More details are given in references [40] and [41].

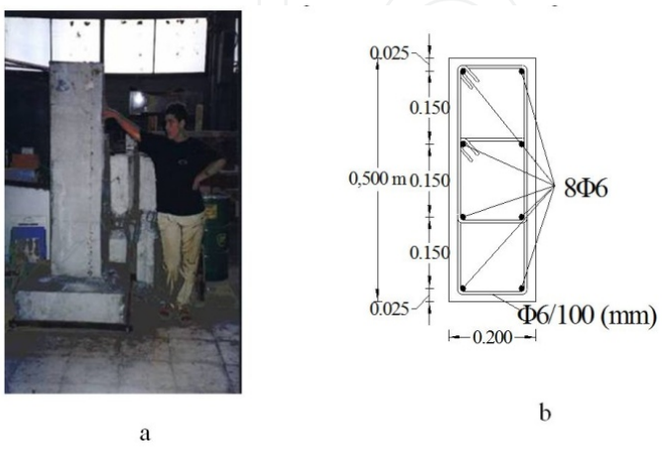

Figure 35. a Pier A. b. Cross-section and reinforcing details of Pier A.

4.1.2. The Loading sequence

The foundation of the specimen was anchored at the strong floor of a reaction frame. The specimen was then subjected to a simultaneous constant vertical load and a cyclic horizontal displacement with increasing amplitude in time, utilizing servo-electronically-controlled dynamic actuators. The frequency of this cyclic displacement was in some tests 0.1Hz whereas in other selected tests it became 1.0Hz. The vertical load was kept constant at 95KN. The horizontal imposed cyclic displacement was applied in 13 groups of continuously increasing amplitude. Each group included 3 full cycles of constant amplitude. This time history of the imposed displacement is depicted in figure 36a. The amplitude in this picture is non-dimensional and is given as a percentage of the final maximum amplitude of this cyclic loading. In the experimental sequence the maximum displacement horizontal amplitude was initially relatively small (2mm); as testing progressed, in subsequent cyclic loading sequences it reached values of 20mm to 25mm. The imposed displacements were measured at the location of the horizontal actuator which was placed at a height of 1400mm from the top of the foundation (figure 36b). Figures 36b and 36c depict this experimental set-up. As can be seen the specimen was placed in the strong reaction frame, having its foundation block, with dimensions in plan 1000mm by 1000mm and 300mm height, fully anchored to the strong floor. The horizontal and vertical actuators, as part of this strong reaction frame, applied the loading sequence described above. Instrumentation was provided in order to measure the variation of the applied horizontal and vertical loads as well as the most important aspects of the displacement field that resulted from the application of these loads to the specimen. The horizontal displacements of the specimens at the top were monitored as well as the displacements of the specimen at the region near the foundation block in order to identify the flexural, and shear deformations as well as the plastic hinge behavior at this part of the specimen. In figure 36b the two vertical sides of the specimen where the CFRP layers were attached are indicated together with the region where the anchoring arrangements were placed as part of the current investigation. Throughout these series of experiments the nominal thickness of the employed CFRP layers was 0.176mm with a given Young's Modulus E=350GPa. The measured maximum axial CFRP strain was approximately 1%. These CFRP layers were placed at these locations

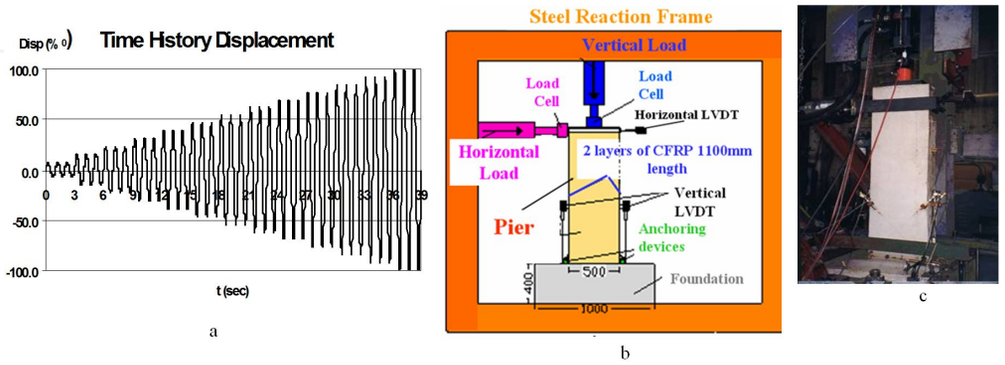

Figure 36. Imposed horizontal displacement. 36b. Experimental set-up. 36c Pier A placed at the strong reaction frame.

http://dx.doi.org/10.5772/51326

4.2. Observed Behavior - Results

4.2.1. The behavior of Pier A

The yield stress of the longitudinal reinforcements was equal to 344.8MPa whereas the concrete strength was equal to 21.2MPa. Based on these mechanical characteristics and the cross-section reinforcing detailing, predictions of the limit-state flexural behavior for this virgin specimen (without CFRP) were obtained in terms of the M-N interaction. The limit-state flexural behavior of a specimen with 2 layers of CFRP attached to both vertical sides of a repaired specimen is also obtained, based on the assumption that the cross-sections under flexure remain plane even with the attachment of the CFRP layers. The development of flexural cracks took place as shown in figure 37. At this horizontal cross-section the measured flexural behavior of Pier A is depicted in figure 38, which presents the variation of the resulting bending moment at this cross-section of the specimen against the rotation of the same cross section,. The rotation was obtained from measurements made by displacement transducers that were placed at the two sides of the pier monitoring the relative vertical displacement between the upper part of the specimen and its foundation block. Additional instrumentation was provided to monitor the rocking or the sliding of the foundation block itself, which proved to be non-significant. The observed maximum bending moment value compares quite well with the corresponding predictions of the limit-state flexure for this cross-section. The red line in these plots represents the corresponding envelope curve.

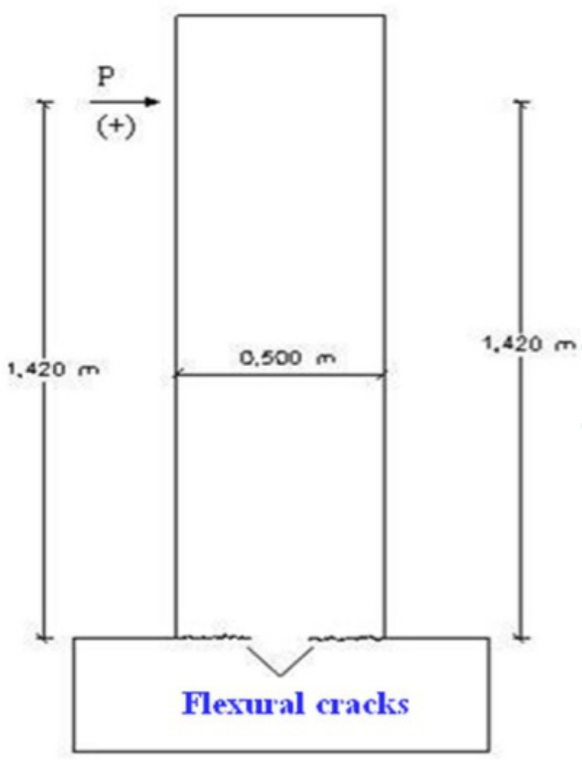

Figure 37. Observed flexural cracks for Pier A.

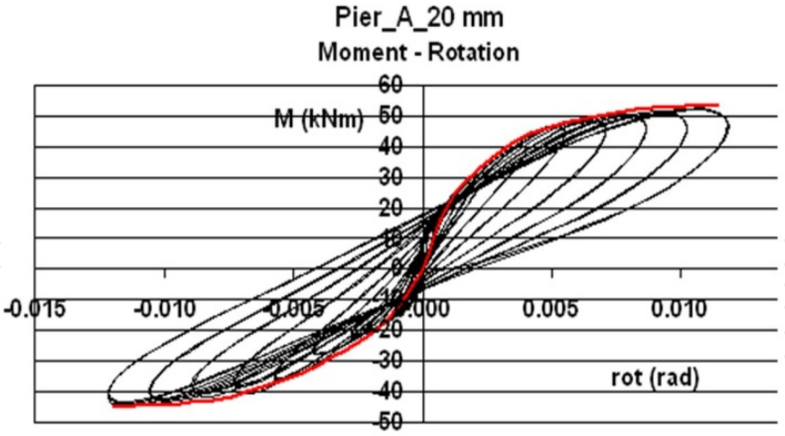

Figure 38. The measured flexural response of Pier A in terms of bending moment - plastic rotation.

4.2.2. Repaired specimen Rep-1 Pier A and observed behavior

The damaged Pier A was repaired in a way depicted by figures 39a,b. The resulting specimen is designated as Rep-1 Pier A. Two layers of CFRP were attached at each vertical side of the pier's cross-section. This attachment extended to a height of 1100mm from the foundation surface as well as at the top surface of the foundation block depicted in figure 39b. Moreover, in order to increase the bond strength between the CFRP layers and the top surface of the foundation block two double T steel sections were placed at these locations. A force normal to the bond surface at this location was applied by bolting these double T steel sections to the foundation block utilizing pre-stressing rods. Due to space limitations no further details are given here.

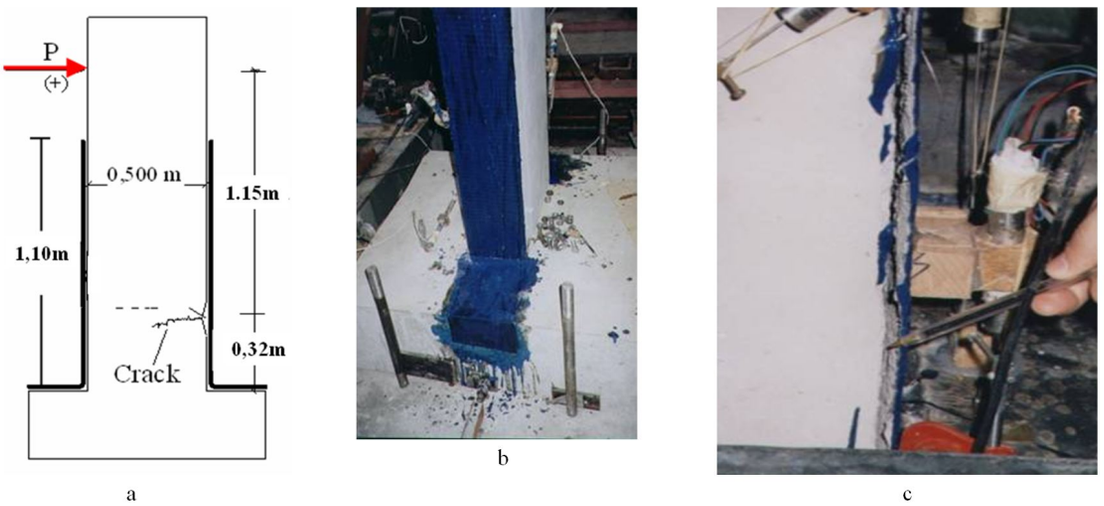

Figure 39. Specimen Rep-1 Pier A. Specimen 39b Rep-1 Pier A, attachment of CFRP layers. 39c Debonding of the CFRP layers from the right side of the repaired specimen Rep-1 Pier A.

http://dx.doi.org/10.5772/51326

4.2.3. Observed Behavior of Specimen Rep-1 Pier A

The loading sequence, described before, was applied to this repaired specimen. During increasing of the imposed horizontal displacement the debonding of the CFRP layer at the right side of the pier occurred as depicted in figure 39c. The obtained flexural behavior is depicted in figure 40 in terms of applied horizontal load against the imposed horizontal displacement at the top of the pier. If this behavior is compared with the corresponding behavior of the virgin specimen Pier A, a modest increase in its bearing capacity of approximately 20% can be observed as a result of the applied CFRP repair scheme, despite the debonding of the CFRP layers. The red line in this figure represents the corresponding envelope curve.

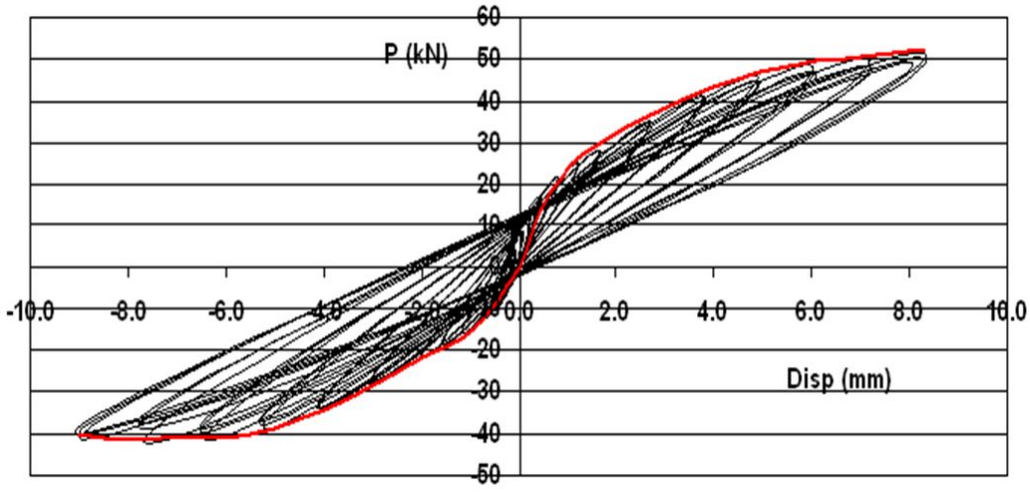

Figure 40. The measured flexural response of Rep-1 Pier A in terms of Horizontal load - Horizontal Displacement.

4.2.4. Repaired specimen Rep-2 Pier A and observed behavior

The damaged Rep-1 Pier A was repaired again in a way which is shown in figures 41a,b. The CFRP layers that were separated from the concrete at the right side of Rep-1 Pier A were reattached, both with the appropriate resin and additional 2mm diameter small bolts of 35mm length; these bolts were spaced at regular 50mm intervals along all the height of the CFRP layer at both sides. Moreover, the edge of the double T steel section neighboring the location of the CFRP layer at the pier-foundation joint was machined to form a curvature so that it provided a relatively uniform contact between the steel section and CFRP layers at this location. The locations of the bolts were first marked and drilled and then the bolts were applied including the corresponding plastic anchoring inserts. The specimen repaired in this way is designated as Rep-2 Pier A.

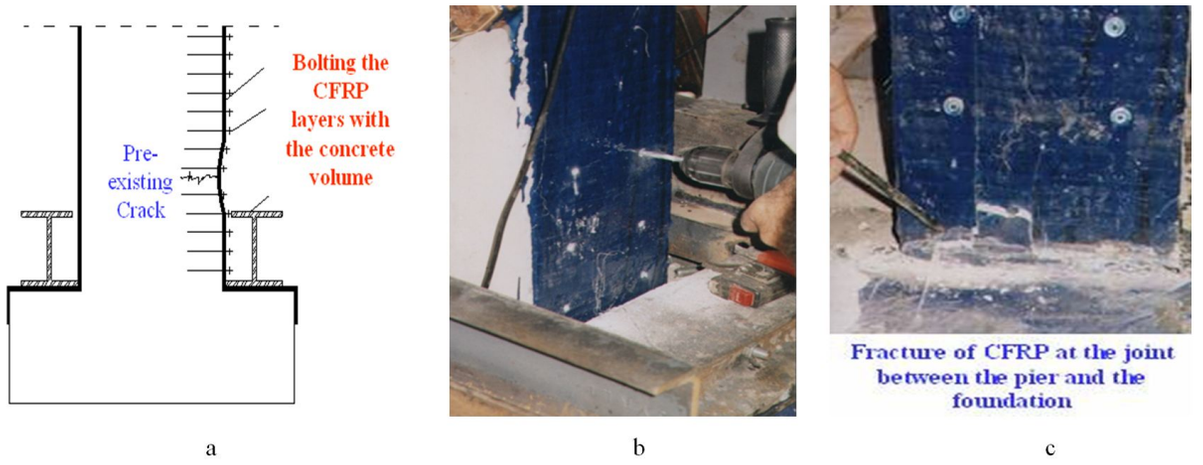

Figure 41. a The repair of specimen Rep-1 Pier A. b. The repair of specimen Rep-1 Pier A. c. Fracture of CFRP for specimen Rep-2 Pier A.

4.2.5. Observed Behavior of Specimen Rep-2 Pier A

The loading sequence, described in section 2, was also applied for this repaired specimen. During the increasing of the imposed horizontal displacement the fracture of the CFRP layers at the right side of the pier occurred as depicted in figure 41c. This fracture occurred at the location where the pier joins the foundation block. Figure 42a presents the variation of the measured horizontal load versus the horizontal displacement, whereas the resulting bending moment against the plastic hinge rotation is plotted in figure 42b. The plastic hinge which was formed during testing specimen Rep-1 was not repaired in any other way, but with the means described before. The fracture of the CFRP layer depicted in figure 41c took place at the same cross section. As was mentioned before the plastic rotation was measured by displacement transducers that were placed at the two sides of the pier. Because of the dislocation of one of these transducers the rotation angle after that was not monitored. This is noted at the bottom left hand side of figure 42b. Despite this lack of rotation measurements after the dislocation, the bending moment capacity remains approximately at the same levels, as deduced from the variation of the horizontal load (figures 42a and 43a). The effectiveness of the applied repair schemes for specimens Rep-1 and Rep-2 can be seen in figures 43a and 43b in terms of envelope curves. In figure 43a the comparison is made in terms of horizontal load – horizontal displacement whereas in figure 43b this is done in terms of bending moment-rotation. As can be seen, the effectiveness of the CFRP layers is inhibited by the debonding of the CFRP layers; thus although a considerable increase is achieved in the bearing capacity, this is not sustained in terms of displacement because of the premature debonding of the CFRP. The improvement of the bonding with the use of the employed bolting scheme for Rep-2 resulted in an increase of the bearing capacity both in terms of load and displacement and resulted in the fracture of the CFRP.

http://dx.doi.org/10.5772/51326

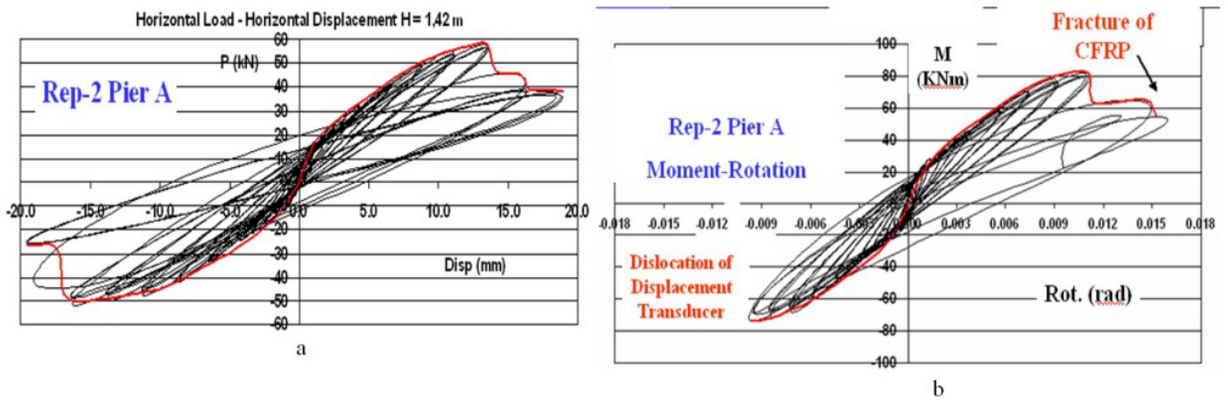

Figure 42. The measured flexural response of Rep-2 Pier A in terms of horizontal load - horizontal Displacement. 42b. The measured flexural response of Rep-2 Pier A in terms of bending moment - plastic rotation.

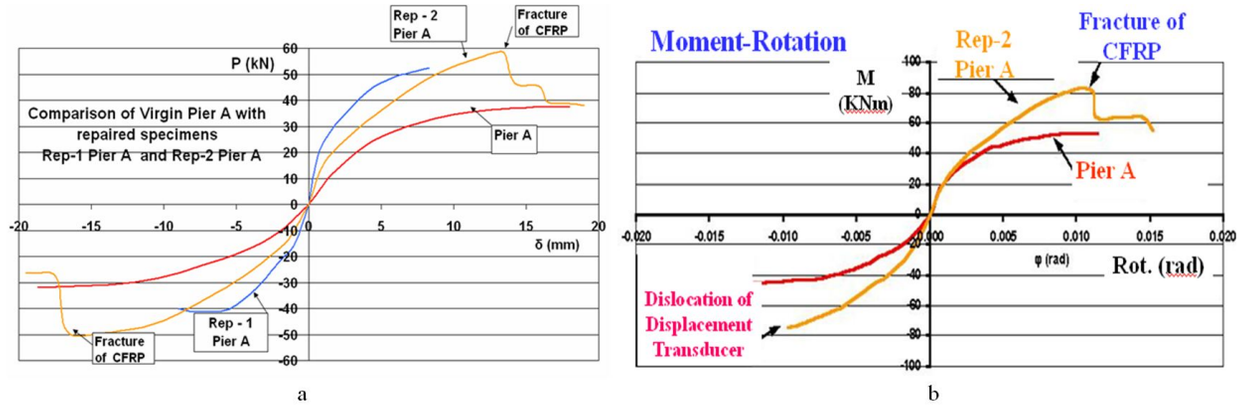

Figure 43. a Comparison of flexural response of repaired Rep-2 Pier A with repaired specimen Rep-1 Pier A and virgin specimen Pier A in terms of Horizontal load – Horizontal displacements. b. Comparison of flexural response of repaired Rep-2 Pier A with virgin specimen Pier A in terms of bending moment - plastic rotation.

From figure 43b the effectiveness of the repair scheme utilized in specimen Rep-2 Pier A can be deduced compared with the virgin specimen Pier A in terms of bending moment - plastic hinge rotation. The achieved increase in bending moment is almost 50% and the flexural behavior in terms of rotation is satisfactory up to the fracture of the CFRP layer at the joint between the pier and the foundation. Comparing the maximum value of the bending moment (83KNm) that was resisted by specimen Rep-2 Pier A with the one predicted (130KNm), as an ultimate bending moment that the cross-section reinforced by the applied CFRP layers can ideally resist, it can be concluded that the fracture of the CFRP did not allow this ideally maximum bending moment value to be reached. One reason for this is the way the anchoring of the CFRP layers at the foundation block is achieved with the utilization of the double T steel sections described before. Despite the machining of the edge of these double T steel sections the development of high stress levels concentrated at the CFRP layers at these locations is the cause of the observed CFRP fracture. Moreover, such an an-

choring scheme is quite impractical for prototype conditions. For these reasons a different anchoring scheme was investigated in order to address both these shortcomings that were found to be critical in the repair schemes investigated so far. This is presented next in a summary form.

4.2.6. Repaired specimen Rep-3 Pier A and observed behavior

Figure 44a depicts the outline of this anchoring scheme and figure 44b depicts the application of this anchoring scheme for repair specimen Rep-3 Pier A, whereby the CFRP layers are folded around a cylinder that is anchored to the foundation [40]. Moreover, in order to avoid the separation (detachment) of the CFRP layers from the sides of the specimen, as observed in specimen Rep-1, the bolting scheme that was used in specimen Rep-3 was further improved by using bolts and washers of larger size (due to space limitations no details are given here). In addition, to avoid the development of shear failure at the bottom part of the pier, three horizontal CFRP closed hoops were attached in this region of the specimen (see figures 44c, 44d and [40], [41], [42]).

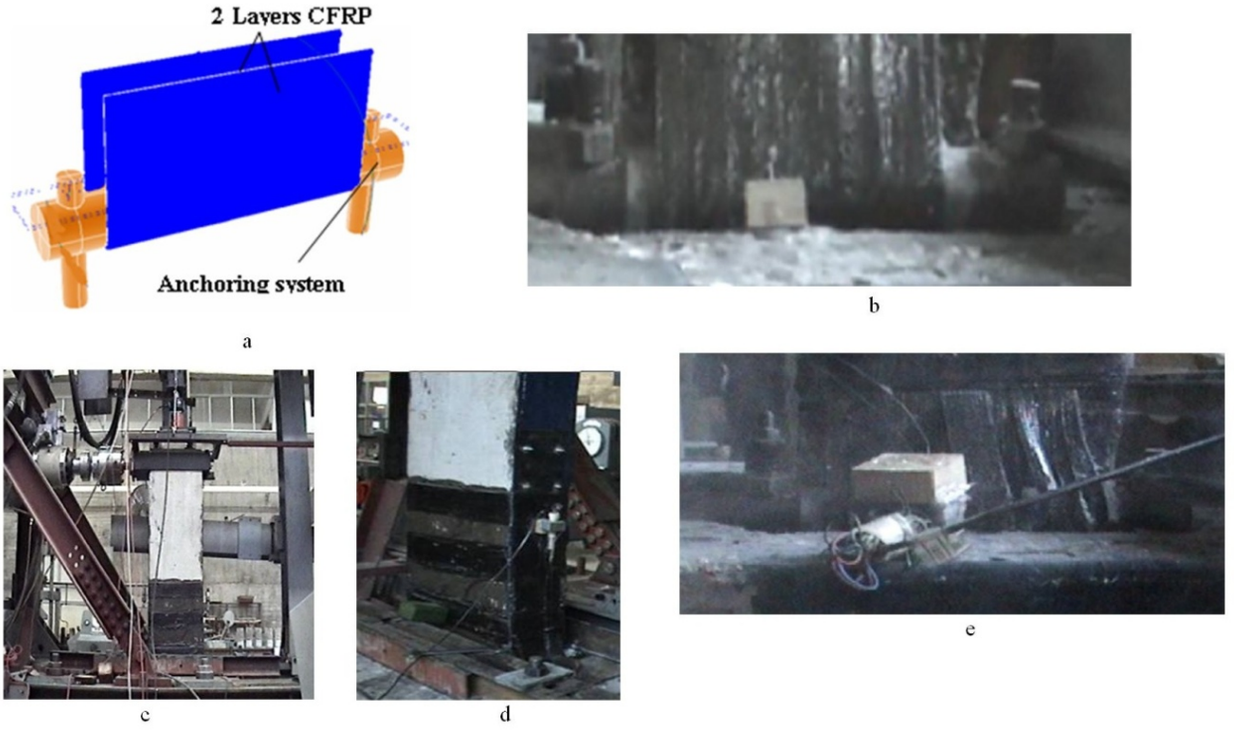

Figure 44. a New anchoring device. b. New anchoring device. c. Specimen Rep-3 Pier A. Figure d. Specimen Rep-3 Pier A. Figure e. Partial fracture of CFRP layers at the cylindrical part of anchoring device

http://dx.doi.org/10.5772/51326

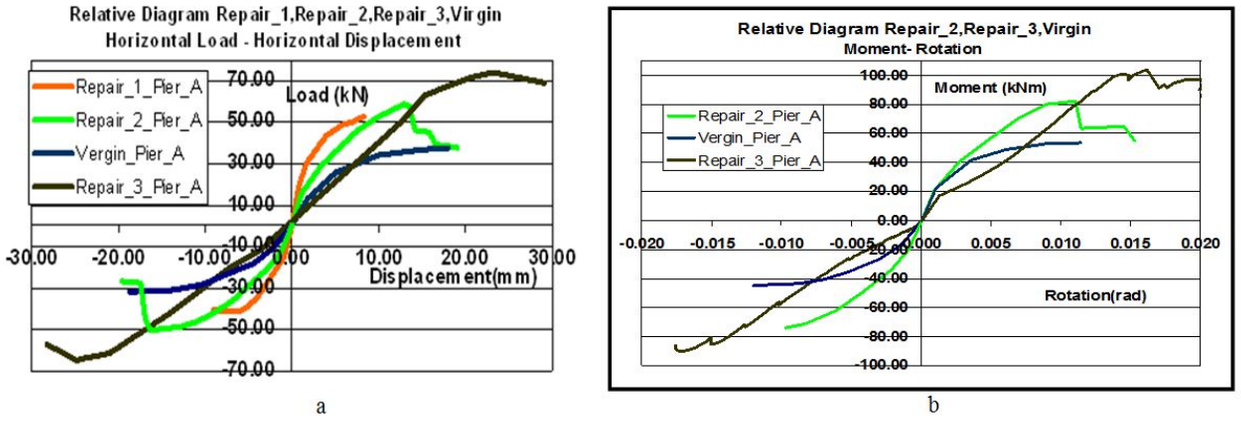

Figure 45. Comparison of flexural response of repaired specimens Rep-3, Rep-2, Rep-1 and virgin specimen. 45b. Comparison of flexural response of repaired Rep-3, Rep-2 and virgin specimens.

4.2.7. Observed Behavior of Specimen Rep-3 Pier A

The loading sequence, described before, was also applied for this repaired specimen. During increasing of the imposed horizontal displacement the partial fracture of the CFRP layer at the right side of the pier occurred as depicted in figure 44e. This fracture occurred at the location where the CFRP layers are folded around the cylindrical part of the anchoring device of figures 44a,b. In figures 45a and 45b the measured flexural behavior in terms of horizontal load-horizontal displacement and bending moment-rotation envelope curve diagrams for repaired specimen Rep-1, Rep-2 and Rep-3 is compared with the coresponding flexural behavior of the virgin specimen Pier A. Due to space limitations the measured full cyclic response for specimen Rep-3 is not included in this presentation. The following observations can be made on the basis of these diagrams. a) The horizontal load and maximum bending moment bearing capacity of the latest repair scheme, namely specimen Rep-3, exhibits an increase of almost 100% when compared with the corresponding bearing capacity of the virgin specimen. b) When this comparison is made between the latest repair scheme Rep-3 and repair scheme Rep-2 the increase is of the order of 25%. Moreover, the new anchoring scheme does not cause an abrupt fracture of the CFRP at the anchoring device. This is reflected in figures 45a and 45b by the fact that the obtained response of specimen Rep-3 extends to relatively large displacement and rotation values. c) A reduction in the initial stiffness appears to be present in specimen Rep-3 when its obtained cyclic response in terms of the envelope curve of figures 45a,b is compared to the corresponding curves of specimen Rep-2 and the virgin specimen. This must be attributed to the fact that most parts of specimen Rep-3 have been subjected to three full loading sequences except the new parts of the CFRP. d) Rep-1 corresponds to the least effective repair scheme due to the debonding of the CFRP layers.

4.3. Concluding Observations

a3. The upgrading of the flexural behavior of vertical R/C structural elements was investigated utilizing the possibility of attaching longitudinal CFRP layers that can be stretched de-

veloping tensile forces externally at the opposite sides of these elements. Critical aspects for their satisfactory performance are the bonding of the CFRP layers as well as the effective transfer of the tensile forces to the foundation block.

b3. The bonding of the CFRP layers at the sides can be improved by bolting schemes that, in this way, increase the cooperation between the CFRP layers and the concrete part.

c3. The transfer of the tensile forces that develop at the CFRP layers to the foundation is a difficult technical problem. Two schemes were tried. The 2nd scheme is more practical and was successful in mobilizing sufficiently the available capacity of the applied CFRP layers in such a way that it resulted in approximately 100% increase in the flexural capacity when compared to the initial flexural capacity of the virgin specimen before the application of the CFRP layers.

d3. The applicability of such an anchoring system must be validated in a more general way before final practical conclusions can be reached.

e3. Such an upgrading of the flexural capacity may lead to the appearance of the shear mode of failure. However, the shear capacity can be increased with relative ease by closed CFRP hoops.

5. Relevant code provisions - Emphasis in the application of FRP strips for shear strengthening

During the last fifteen years numerous researchers ([12], [18], [29], [34]) have proposed different approaches for predicting the behavior of FRPs when they are used for strengthening structural members. Several design guidelines and code provisions adopted some of the proposed approaches. More specifically, the approach of Triantafillou and Khalifa [33] has been adopted by the American Code ACI 440 [11] whereas the model of Chen and Teng ([18], [25]) is utilized in the Greek Code of Interventions [6]. Eurocode 8 part 3 ([7]) follows the guidelines of FIB [8]. In the following paragraphs the aforementioned three Codes are discussed with particular emphasis being given to the application of FRP strips for shear strengthening. All codes recommend a limit-state tensile force that a cross-section (A_{FRP}) of an FRP sheet can sustain. This limit-state tensile force is obtained through equation 2:

$$V_{FRP} = \frac{A_{FRP} \cdot \varepsilon_{FRP} \cdot E_{FRP}}{\varphi} \quad (2)$$

Where: V_{FRP}: Limit-state tensile force of the FRP strip, φ: safety factor, A_{FRP}: cross section area of a strip of FRP

ε_{FRP}: developed axial strains on the FRP strip, E_{FRP}: modulus of elasticity of the FRP strip

The various codes recommend the application of Equation 2 by defining various values for the safety factor (φ) and the limit-state axial strain value (ε_{FRP}). These values vary according to the application depending on whether the predicted FRP contribution is for shear, flexure

http://dx.doi.org/10.5772/51326

or confinement. In doing so, the basic factors that are varied among the Codes are the safety factor and the allowable developed strain on FRP. Table 7 presents the maximum allowable ε_{FRP} values and the recommended safety factor (φ) values according to ACI 440, Eurocode part 3, and the Greek Code for structural interventions, when anchoring is used in the transfer of FRP strip forces.

Code	Max allowable ε_{FRP}		φ
	Flexure	Shear	
ACI 440 [11]	0.9 ε^*_{nom}	0.4 %	1.24 - 1.47
Eurocode 8 (part3) 7	-	0.6 %	1.5
Greek Code of Interventions 6	$\varepsilon^*_{nom} / 2 < 1.5\%$	$\varepsilon^*_{nom} / 2 < 1.5\%$	1.25

Table 7. Maximum allowable developed strains ε_{FRP} and proposed safety factors φ when anchoring is used.Where: ε^*_{nom}: max strain from manufacturer

The allowable limit-state axial strains (ε_{FRP}) value defined by the various codes also depend upon the way the FRP sheets are attached upon the structural elements in need of strengthening. According to all code provisions, there are two basic ways of attaching FRP sheets on structural elements. First, they can be attached using an anchoring device or they can be fully wrapped around the structural element. Secondly, they can simply be attached on the surface of the structural element through an organic or inorganic matrix in an open loop U-shaped without any anchoring. When the simple attachment is used without anchoring the debonding mode of failure prevails, whereas when FRP sheets are combined with an anchoring device or when they are fully wrapped around a column or a beam, fracture of FRP's occurs. The debonding mode of failure poses a limitation to the FRP axial strains and stresses. This limitation is reflected in all three Codes through a factor (usually designated as k_v), that takes values less than 1. This reduction factor depends on the recommended value of the attachment FRP length (effective attachment length). Table 8 lists the basic formulae included in the various codes for calculating this effective attachment length. The most important factor in calculating the effective attachment length is the determination of bond strength, which is not easily obtained since it depends on the actual concrete tensile strength and the state of the surface where the FRP is attached; both these parameters can easily vary even for the same structural element.

When the attachment of FRP sheets is combined with an anchoring device a more reliable transfer of forces can be achieved thus resulting in an equally reliable design of the relevant strengthening scheme. Moreover, since the prevailing mode of failure is the fracture of the FRP's, when anchoring of the FRP strips is used, the exploitation of the material of the FRP sheets is enhanced by reaching higher values of axial strains than for the cases governed by the debonding mode of failure. Under all circumstances the maximum allowable strains should not exceed the value presented in table 7. All codes demand the use of a safe anchoring device that would allow the fracture of FRP sheets without proposing any calculations

for the safe design of these anchoring devices. In any case, equation (3) describes this condition for the bearing capacity of a permissible anchoring device

Code	Effective Length (Le)	
ACI 440 [11]	$L_e = \frac{23300}{(nt_f E_f)^{0.58}}$	where n: number of FRP layers t_f: thickness of FRP E_f: Modulus of elasticity
Eurocode 8 (part3) [7]	$L_e = \sqrt{\frac{E_f \cdot t_f}{\sqrt{4 \cdot \tau_{max}}}}$	where E_f: Modulus of elasticity t_f: thickness of FRP τ_{max}: bond strength
Greek Code of Interventions [6]	$L_e = \sqrt{\frac{E_j t_j}{2 f_{ctm}}}$	where E_j: Modulus of elasticity t_j: thickness of FRP f_{ctm}:tensile concrete strength

Table 8. Calculation of effective length. Where V_{FRP}: total force received by FRP, $V_{anchoring\ device}$: total strength of the anchoring device.

$$V_{FRP} \leq V_{anchoring\ device} \tag{3}$$

6. Special study for anchoring FRP strips

In this section results from a recent research effort conducted at the Laboratory of Strength of Materials and Structures of Aristotle University will be briefly presented and discussed ([13], [42]). This research aimed to investigate the effectiveness of a specific FRP strip anchoring device by utilising a number of small concrete prismatic specimens, that can house such an FRP strip with sufficient width and length. In all, twelve (12) specimens were investigated. For six specimens no surface preparation of the concrete specimen was applied when attaching the FRP layers, whereas six other specimens had their surface treated according to construction guidelines. CFRP layers were attached to all specimens ([28], [43]). The use of the anchoring device was utilised on three (3) specimens with treatment preparation and on three specimens without such treatment. All the concrete prisms were fabricated using the same concrete mix and the same internal reinforcement, which was used to prohibit any accidental failure. The measured cylinder strength of the concrete was equal to 22 MPa. The properties of the used CFRP are listed in Table 9, as given by the manufactures.

http://dx.doi.org/10.5772/51326

Material	Type / Name	Modulus of Elasticity (GPa)	Thickness of Layer (mm)	Ultimate strain
CFRP	SikaWrap 230 C/45	234	0.131	0.018

Table 9. Properties of the used FRP sheets.

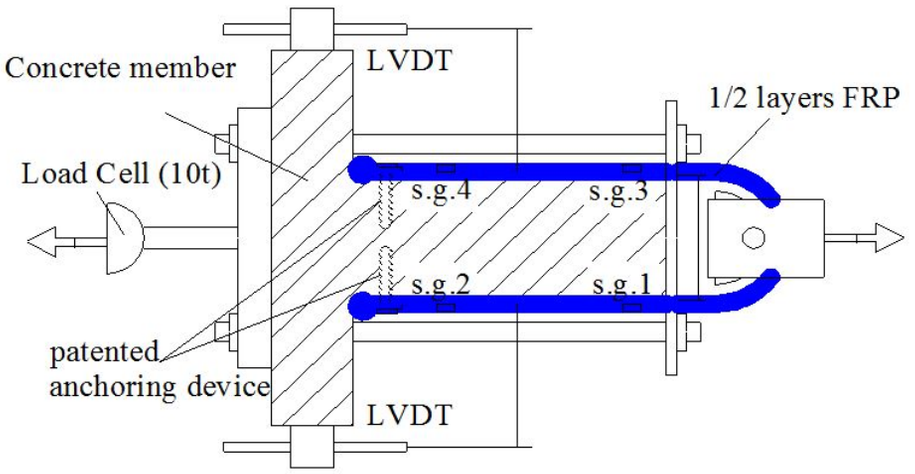

Figure 46. Experimental Set-up.

The loading arrangement is depicted in figure 46, whereby the tensile force is directly applied in the axis of symmetry at the right part of the FRP strips that forms an open hoop at this location; the other two sides of the FRP strip are bonded in a symmetric way on the top and bottom side of the concrete prism, as shown in this figure. When anchors were employed they were added at these locations (ends of the FRP strips). Despite the symmetry of this test set-up, instrumentation was provided that was able to record symmetric as well as asymmetric response of the specimen, especially during the initiation and propagation of the debonding process. During testing, the applied load is measured together with the longitudinal (axial) strains at four different locations of the external surface of the FRP strip, as indicated in figure 46 (s.g.1 to s.g.4), in order to calculate the stress field that develops at the FRP layer before and during the debonding.

Moreover, the relative longitudinal displacement between the concrete prism and the FRP surface is also monitored using four displacement transducers that are properly attached to the specimen, as indicated in this figure, in order to record the initiation and propagation of the debonding of the FRP. The used anchoring device was developed at the Laboratory of Strength of Materials and Structures of Aristotle University of Thessaloniki in Greece and it is patented with patent number WO2011073696 [42]. Figure 47 presents some details of this device. The tested specimens with their details are listed in table 10 together with their code names. The first letter C in the code name denotes a carbon fiber reinforcing polymer strip. (CFRP). The type of surface preparation is denoted by the second letter of the code name (S for smooth surface, R for rough surface; the type of anchor is denoted by the third letter of the code name (N for no anchor and P for patented anchoring device). Moreover, the num-

ber of layers of these strips is denoted by the fourth character of the code name (1 for one layer and 2 for two layers). The tests were conducted using a 1000 kN capacity hydraulic piston. The measurements of load, displacements and strains were recorded using an automatic data acquisition system.

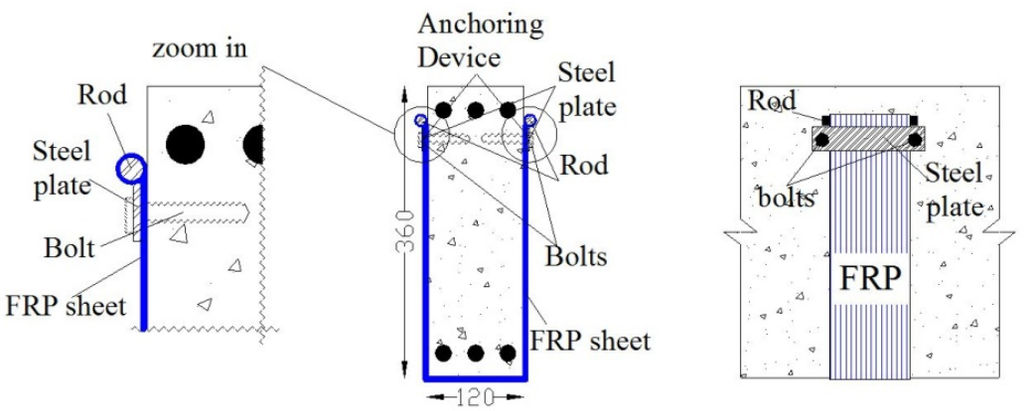

Figure 47. Patented Anchoring Device (WO2011073696).

Spec. Name	Material Type	Number of Layers	Surface Type	Anchor Type	No. of specimens	Bolt Type
CSN1	CFRP	1	smooth	no	3	no
CRN1	CFRP	1	rough	no	3	no
CSP2	CFRP	2	smooth	patented	3	2XHUS by Hilti
CRP2	CFRP	2	rough	patented	3	2XHUS by Hilti

Table 10. Details of Specimens.

Spec. Name	Anchor Type	Max Load (kN)	Failure Mechanism	Load at Debonding (kN)	Max Strain (μStrain) s.g.1	Max Strain (μStrain) s.g. 3	Material Exploitation M_e	Load from Strain (kN)
CSN1	no	27.9	debonding	27.9	5400	5400	0.30*	32.5
CRN1	no	42.7	debonding	42.7	6335	7215	0.38*	40.8
CSP2h	patented	112.8	CFRP fracture	30	9810	8320	0.50	109.2
CRP2h	patented	103.0	CFRP fracture	40	7220	9330	0.46	99.7

Table 11. Summary of experimental results. * Specimens with only one CFRP layer. If for these specimens a second CFRP layer was added without anchor, due to the debonding failure, no increase in the maximum load and maximum strain can be achieved. Consequently, in such a case the exploitation ratio value would be half the values listed in this table.

http://dx.doi.org/10.5772/51326

Experimental Results and Discussion: The summary of the experimental results is listed in table 11. In this table, the observed failure mechanism is listed together with the corresponding value of the ultimate measured load as well as the value of the load recorded at the initiation of debonding. Moreover, the maximum strain values measured by the strain gauges at locations 1 and 3 on the FRP strip surface are also listed. The average value of these maximum FRP strains was utilised to calculate indirectly the load sustained by the FRP strips taking into account their total cross-sectional area and the value of the Young's modulus, listed in table 10. Finally, the material exploitation indicator (M_e) is given in the same table as the ratio of the maximum measured strain by the ultimate strain value provided by the manufacturer (Table 10).

For specimens CSN1 having non-prepared surfaces, an average ultimate load was found equal to 27.9 kN. The equivalent ultimate load value when prepared contact surfaces were used, specimens CRN1 and SRN1, was 41 kN. Thus, the proper preparation of the contact surface resulted in a 46% increase of the ultimate load. This increase that is attributed to the surface preparation was observed when no anchoring device was utilized. The employed surface preparation needs at least twice as much time as when no surface preparation is made.

When an anchoring device is employed, it can be seen that preparation of the concrete contact surface is of no significance (see the ultimate load values of the anchored specimens of table 11 and those of debonding). In all tested cases the ultimate load is greater than the load at debonding. Thus, when using an effective anchoring device, the cost of properly treating the contact surface can be avoided.

The load at debonding for those specimens whose surfaces were not specially treated had a value approximately equal to 30 kN with small deviations. Similarly, the load at debonding for those specimens whose surfaces were specially treated had a value approximately equal to 40kN with small deviations. When an anchoring device is utilized the ultimate capacity increases from 28 kN to 112.8 kN for the set of specimens strengthened with CFRP. This represents a fourfold increase in the value of ultimate load.

Finally, when the patented anchoring device was applied for specimens CSP2h, CRP2h, a significant increase in the bearing capacity was observed. This time the performance of the anchoring device was very satisfactory and the observed failure was that of the fracture of the FRP strips for all these specimens. Figure 6 depicts such a failure mode for specimen SSP2b (see also table 11).

In order to discuss the observed behavior in terms of exploitation of the high strength of the FRP materials the following procedure was used. As already mentioned, a material exploitation indicator was found (M_e) as the ratio of the maximum measured strain values (average of the two sides, Table 3) for each specimen over the ultimate strain values as they are measured for the used FRP materials (see table 9). These material exploitation indicator values are also listed in Table 11, having ideally as an upper limit the value of 1. As can be seen in this table, the highest M_e value during the present experimental sequence reaches the value 1 and this was achieved by the specimen that utilises the patented anchoring device together with two layers of CFRP strips. As expected, debonding of the FRP strips or failure of the

anchoring device results in relatively low values of the material exploitation indicator M_e. (0,60 and 0,79) This research effort is in progress experimenting with various alternative anchoring details.

Figure 48. Detail of the anchoring device and the fracture of the CFRP strip when such an anchoring device is employed.

6.1. Concluding Observations

a4. Proper preparation of the contact surface between the FRP strips and the concrete face resulted in a 46% increase of the ultimate load. This increase that is attributed to the surface preparation was observed when no anchoring device was utilized. The employed surface preparation needs at least twice as much time as when no surface preparation is done.

b4. When an anchoring device is employed, it can be seen that preparation of the concrete contact surface is of no significance. With the proper anchoring device the ultimate capacity increases four times.

c4. It is important to properly detail the anchoring device in order to drive the mode of failure to the fracture of the FRP strip rather than the failure of the anchor thus exploiting the high tensile strength FRP potential.

d4. The highest value of the FRP material exploitation indicator was achieved in the specimen that utilises the anchoring device patented by Aristotle University together with two layers of CFRP strips.

e4. As expected, debonding of the FRP strips or failure of the anchoring device results in relatively low values of the material exploitation indicator M_e. This research effort is in progress experimenting with various alternative anchoring details.

7. Basic qualification tests for fiber reinforcing polymers (FRP) sheets to be used in dealing with earthquake structural damage.

In what follows, a brief description is given of basic qualification tests to be performed with FRP sheets used in repair / strengthening schemes of R/C structural elements in the framework of earthquake structural damage. As already discussed in sections 5 and 6, the main

http://dx.doi.org/10.5772/51326

critical parameters for such use of FRP sheets are: a) the modulus of elasticity, b) the maximum axial strain and c) the effective thickness of these sheets. These properties are usually provided as technical specification data by the manufacturers of these materials. Moreover, the manufacturers of the FRP sheets for this type of application also provide technical information on the organic or inorganic matrices that are compatible with the relevant FRP sheets and the type of material surface of the structural element to which these sheets are to be externally applied. Finally, the technical information of the manufacturers as well as the relevant code guidelines include preparatory actions which must be taken before the FRP sheets are applied, such as concrete surface preparation, rounding of corners and proper application of the matrices together with the FRP sheets prohibiting the formation of any air pockets. In case the tensile characteristics of the FRP sheets must be confirmed, specimens of the FRP material must be taken in order to define the modulus of elasticity (E), the Poisson's ratio (ν), the tensile strength and the maximum tensile failure strain (ε_m). These tests are performed following the appropriate specifications of the relevant standard (e.g. European Standard EN ISO 527-5: 1997).

During the various experimental sequences that were presented in the preceding sections 2, 3 and 4 the employed FRP sheets were tested in order to verify their basic tensile characteristics. Selective measured values are reported in the relevant sections in brief (see subsections 2.2.2, 3.1.2 and 4.1.2). For all tests reported in sections 2, 3 and 4 the FRP sheets were attached to the reinforced concrete specimens using the same organic matrix. This was a two part, solvent free, thixotropic epoxy based impregnating resin / adhesive. The density of this epoxy resin is 1.31 kg/l and its average viscosity is approximately 7.000 mPas. The Thermal Expansion Coefficient is equal to 45 x 10-6 per °C, its tensile strength according to DIN 53455 is 30 Mpa, the Young's Modulus is 4500 Mpa and the ultimate elongation is 0.9%. There is a manufacturers warning that this product is not suitable for chemical exposure.

7.1. Bond Strength between CFRP layers and Concrete Substrate.

Another property of interest is the bond strength between the FRP sheets and its matrix with the surface of the structural member, especially when the FRP sheets are not accompanied by the appropriate anchoring, as discussed in the preceding sections. There are certain bond strength tests aiming to insure that the debonding mode of failure does not occur between the matrix and the FRP sheet (e.g. European Standard EN ISO 1542: 1999). However, when designing for the debonding limit-state use is made of the tensile strength of the concrete substrate instead of this bond strength. A special investigation was performed at the Laboratory of Strength of Materials and Structures of Aristotle University aiming at measuring directly this bond strength of the employed CFRP sheets attached with the named above epoxy resine to the concrete substrate. Figure 49a depicts this simple test aimed at measuring the bond strength between the employed CFRP layers and the concrete surface (ref. [40], [41]). Figure 49b depicts the obtained results together with a best-fit linear variation of the bond strength (τ) versus the applied normal stress ($\sigma_{\varepsilon\gamma\kappa}$). As expected, a modest increase can be obtained in the bond strength (τ) between the CFRP layers and the concrete surface if a

normal stress ($\sigma_{\varepsilon\gamma\kappa}$) increase is applied at the bond surface. This was partly made use of in the various anchoring schemes employed in sections 2, 3 and 4.

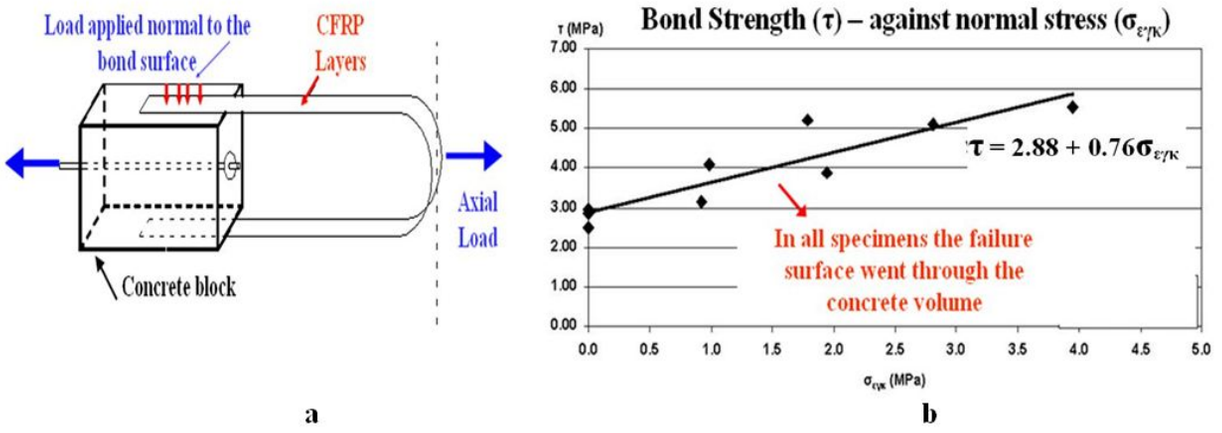

Figure 49. a Test for estimating the bond between CFRP layers and concrete surface and b obtained results.

7.2. Cost estimates

From a comparative study of data dealing with typical cases of repair and strengthening of R/C structural elements with conventional methods (jacketing with gunite or cast-in-place R/C concrete) versus CFRP based strengthening schemes the following constitute the average findings. The cost of a fully wrapped CFRP strengthening scheme when compared to a cast-in-place jacketing, represents an increase of approximately 20% to 30%. However, when a jacketing strengthening scheme with gunite (shotcrete) is applied instead of FRP's the cost increase is of the order of 30% to 40%. If the CFRP repair / strengthening solution does not include full wrapping the above cost increase is expected to be reduced.

8. Conclusions

1. This presentation dealt with repair and strengthening schemes of earthquake damaged reinforced concrete (R/C) structural elements utilizing externally attached fiber reinforcing plastics (FRP's). Such strengthening schemes were studied when applied to slabs, beams and vertical structural members. The success of such an upgrading scheme was discussed together with its limitations on the basis of a series of relevant experimental results.
2. One of the main limitations results from the way the tensile forces which develop on these FRP sheets can be transferred. When the transfer of these forces relies solely on the interface between the FRP sheet and the external surface of the reinforced concrete structural elements, the delaminating (debonding) mode of failure of these sheets occurs, due to the relatively low value of either the ultimate bond stress at this interface or

http://dx.doi.org/10.5772/51326

the relatively low value of the tensile strength of the underlying concrete volume. This mode of failure is quite common and it occurs in many applications well before the corresponding FRP sheets develop tensile axial strains in the neighborhood of values mentioned before as design limit axial strains (approximately of the order of 1%).

3. Alternative ways of transferring these tensile forces, apart from the simple attachment, in order to enhance the exploitation of the FRP material potential have been also presented and discussed based on experimental evidence from ongoing research at Aristotle University.

Acknowledgements

Partial financial support for this investigation was provided by the Hellenic Earthquake Planning and Protection Organization (EPPO), which is gratefully acknowledged.

Author details

George C. Manos* and Kostas V. Katakalos

*Address all correspondence to: gcmanos@civil.auth.gr

Laboratory of Experimental Strength of Materials and Structures, Department of Civil Engineering, Aristotle University of Thessaloniki, Greece

References

[1] Papazachos, B. C. (1990). Seismicity of the Aegean and the Surrounding Area. *Tectonophisics*, 178, 287-308.

[2] Manos, G.C. (2011). Consequences on the urban environment in Greece related to the recent intense earthquake activity. Int. Journal of Civil Eng. and Architecture Dec Serial No. 49) , 5(12), 1065-1090.

[3] Paz, M. (1994). International Handbook of Earthquake Engineering: "Codes, Programs and Examples". edited by Mario Paz, Chapter 17. , Greece by G.C. Manos, Chapman and Hall 0-41298-211-0

[4] Pauley, T., & Priestley, M. J. N. (1992). Seismic Design of Reinforced Concrete and Masonry Structures. J. Wiley & Sons, INC USA.

[5] Organization of Earthquake Planning and Protection of Greece (OASP),. (2001). *Guidelines for Level- A earthquake performance checking of buildings of public occupancy», Athens*.

[6] Organization of Earthquake Planning and Protection of Greece (OASP), (2011). Guidelines for Retrofitting in Reinforced Concrete Buildings, Athens.

[7] Eurocode-8. (2004). Design of structures for earthquake resistance- Part 2: Bridges, DRAFT. 2004, *European Committee for Standardization* [3].

[8] F.fF. I. B. I.S. C. (2001). Externally Bonded FRP Reinforcement for RC Structures. " in Bulletin 14, f.T.G. 9.3, Editor. , 165.

[9] Greek Code for the Design of Reinforced Concrete Structures" (2000). in Greek).

[10] Provisions of Greek Seismic Code. (2000). *OASP, Athens, December 1999. Revisions of seismic zonation introduced in 2003*.

[11] ACI, (2008). Guide for the Design and Construction of Externally Bonded FRP Systems for Strengthening Concrete Structures (ACI 440.2R-08). in ACI 440.2R-08 American Concrete Institute: Farmington Hills , 45.

[12] Bakis, C., et al. (2002, May). Fiber-Reinforced Polymer Composites for Construction-State of the Art Review'. *Journal of Composites of Construction, ASCE*.

[13] Katakalos, K., Manos, G. C., & Papakonstantinou, C. G. (2012). Comparison between Carbon and Steel Fiber Reinforrced Polymers with or without Ancorage. ", 6th International Conference on FRP Composites in Civil Engineering Rome

[14] Manos, G. C., Kourtides, V., & Matsukas, P. (2007). Investigation of the flexural and shear capacity of simple R/C beam specimens including repair schemes with fiber reinforced plastics. FRPRCS-8 World Conference, Greece, July 16-18 2007

[15] Nanni, A. (1995). Concrete repair with externally bonded FRP reinforcement. *Concrete International*, 17(6), 22-26.

[16] Teng, J. G., Chen, J. F., Smith, S. T., & Lam, L. (2002). FRP strengthened RC structures. Chichester: John Wiley and Sons.

[17] Papakonstantinou, C. G., & Katakalos, K. . (2009). . Flexural Behavior of Reinforced Concrete Beams strengthened with a hybrid retrofit system. Structural Engineering and Mechanics Techno Press 31-5

[18] Chen, J. F., & Teng, J. G. (2003). Shear Capacity of Fiber-Reinforced Polymer-Strengthened Reinforced Concrete Beams: Fiber Reinforced Polymer Rupture. Journal of Structural Engineering May 1 ASCE, 5 , 129(5), 615-625.

[19] Papakonstantinou, C. G., Katakalos, K., & Manos, G. C. (2012). Reinforced Concrete T-Beams Strengthened in Shear with Steel Fiber Reinforced Polymers. Paper presented at 6th International Conference on FRP Composites in Civil Engineering, Rome.

[20] Chen, J. F., & Teng, J. G. (2001). Anchorage strength models for FRP and steel plates bonded to concrete. *Journal of Structural Engineering, ASCE*, 127(7), 784-791.

http://dx.doi.org/10.5772/51326

[21] Lamanna, A. J., Bank, L. C., & Scott, D. W. (2004, May/June). Flexural strengthening of R/C beams by mechanically Attaching FRP strips. *Journal of Composites of Construction, ASCE*, 203-210.

[22] Lee, J. H., Lopez, M. M., & Bakis, C. E. (2007, July). Flexural Behavior of reinforced concrete beams strengthened with mechanically fastened FRP strip. Paper presented at FRPRCS-8, World Conference,, University of Patras.

[23] Paterson, J., & Mitchell, D. (2003, May). Seismic Retrofit of Shear Walls with Headed Bars and Carbon Fiber Wrap. *Journal of Structural Engineering, ASCE*, 606-614.

[24] Manos, G. C., & Papanaoum, E. (2009, June). Earthquake Behavior of a R/C Building Constructed in 1933 before and after its Repair. *STREMAH, Tallin*, 22-24.

[25] Chen, J. F., & Teng, J. G. (2003). Shear capacity of FRP strengthened RC beams: FRP debonding. *Construct Build Mater*, 17(1), 27-41.

[26] Ekenel, M., Rizzo, A., Myers, J. J., & Nanni, A. ". (2006, September/October). Flexural Fatigue Behavior of Reinforced Concrete Beams Strengthened with FRP Fabric and Precured Laminate Systems. *Journal of Composites of Construction, ASCE*, 433-442.

[27] Khalifa, A., & Nanni, A. (2002, April). Rehabilitation of rectangular simply supported RC beams with shear deficiencies using CFRP composites. *Construction and Building Materials*, 16(3), 135-146.

[28] Manos, G. C., Katakalos, K., & Papakonstantinou, C. G. (2011). Shear behavior of rectangular beams strengthened with either carbon or steel fiber reinforced polymers. *Applied Mechanics and Materials (Trans Tech Publications)*, 82, 571-576.

[29] Triantafillou, T. C., & Antonopoulos, C. P. (2000). Design of concrete flexural members strengthened in shear with FRP. Journal of Composites for Construction November ASCE., 4(4)

[30] Kani, G. N. J. (1966, Jun). Basic Facts Concerning Shear Failure. *J. ACI*, 63, 675-692.

[31] Zararis, P. (2002). Reinforced Concrete. Kyriakides Editions, Thessaloniki (in Greek).

[32] Zsutty, T. C. (1968, November). Beam Shear Strength Prediction by Analysis of Existing Data. *Journal ACI*, 65, 943-951.

[33] Triantafillou, A. (2003). Software for the design of reinforced concrete elements strengthened with fibre reinforced polymers FRP. (in Greek).

[34] Pantazopoulou, S. J., Bonacci, J. F., Sheikh, S., Thomas, M. D. A., & Hearn, N. (2001). Repair of corrosion-damaged columns with FRP wraps. *Journal of Composites for Construction*, 5(1), 3-11.

[35] Tastani, S. P., Pantazopoulou, S. J., et al. (2006). Limitations of FRP Jacketing in Confining Old-Type Reinforced Concrete Members in Axial Compression. Journal of Composites for Construction February 1,. ASCE., 10(1)

[36] Manos, G. C., & Kourtides, V. (2007, July 16-18). Retrofitting of long rectangular R/C Cross-Sections with Partial Confinement employing Carbon Fiber Reinforcing Plastics. Paper presented at FRPRCS-8 Conf., Greece. (128).

[37] Tsonis, G. (2004). Seismic Assessment and Retrofit of Existing Reinforced Concrete Bridges. Ph.D. Thesis, Politecnico di Milano.

[38] Kawashima, K. (2000). Seismic performance of RC bridge piers in Japan: an evaluation after 1995 the Hyogo-ken nanbu earthquake. *Prog. Struct. Engng Mater*, 2, 82-91.

[39] Pinto, A. V. (1996, November). Pseudodynamic and Shaking Table Tests on R.C. Bridges. *ECOEST PREC*8 R* [8].

[40] Manos, G. C., Katakalos, K., Kourtides, V., & Mitsarakis, C. (2007, July). Upgrading the Flexural Capacity of a Vertical R/C Member Using Carbon Reinforcing Plastics Applied Externally and Anchored at the Foundation. Paper presented at FRPRCS-8 World Conference.

[41] Manos, G. C., Katakalos, K., & Kourtides, V. (2008). Study of the anchorage of Carbon Fiber Plastics (CFRP) utilized to upgrade the flexural capacity of Vertical R/C members. Paper presented at 14WCEE, Beijing, CHINA.

[42] Manos, G.C., Katakalos, K., & Kourtides, V. (2011). Construction structure with strengthening device and method. European Patent Office, Patent A1) —2011-06-23(WO2011073696)

[43] Manos, G.C., Katakalos, K., & Kourtides, V. (2011). The influence of concrete surface preparation when fiber reinforced polymers with different anchoring devices are being applied for strengthening R/C structural members. *Applied Mechanics and Materials*, 82, 600-605.